

University of Alberta

**Identification of Atomistic Mechanisms for Grain Boundary Migration in
[001] Twist Boundaries: Molecular Dynamics Simulation**
by

Xinan Yan

A thesis submitted to the Faculty of Graduate Studies and Research
in partial fulfillment of the requirements for the degree of

Master of Science
in
Materials Engineering

Chemical and Materials Engineering

©Xinan Yan
Fall 2009
Edmonton, Alberta

Permission is hereby granted to the University of Alberta Libraries to reproduce single copies of this thesis and to lend or sell such copies for private, scholarly or scientific research purposes only. Where the thesis is converted to, or otherwise made available in digital form, the University of Alberta will advise potential users of the thesis of these terms.

The author reserves all other publication and other rights in association with the copyright in the thesis and, except as herein before provided, neither the thesis nor any substantial portion thereof may be printed or otherwise reproduced in any material form whatsoever without the author's prior written permission.

Examining Committee

Hao Zhang, Chemical and Materials Engineering

Tian Tang, Mechanical Engineering

Adrian Gerlich, Chemical and Materials Engineering

To my mother,Zou Mingfang, my father Yan,Zhicheng and my wife, Liu Man

Abstract

In this thesis, molecular dynamics simulations were performed to characterize the atomic motions governing grain boundary migration in a series of [001] twist boundaries. Particularly, migrations of a $\theta=36.87^\circ$ $\Sigma 5$, a $\theta=22.63^\circ$ $\Sigma 13$ and a $\theta=40.23^\circ$ general high angle [001] twist boundaries driven by stored elastic energy in fcc Ni were investigated. Atomic motions during migration were identified as the combination of single atom jump and string-like cooperative atomic motions. The simulation results confirmed that the collective 4-atom shuffle motion was the rate controlling atomic motion during the migration of $\Sigma 5$ twist boundary. As grain boundary local symmetry decreasing, string-like cooperative atomic motions became increasingly important. Eventually, both random single atom jump and string-like cooperative motions became dominant during the migration of general non- Σ twist boundary. Furthermore, simulations showed that activation energy for grain boundary migration was well correlated with the average string length occurring within boundary.

Acknowledgements

I would like to be extremely grateful to my supervisor, Prof. Hao Zhang, for his guidance and support in this study. His precise academic manor in every single detail sets an excellent example for my current academic research and future industrial career development. He always provides me valuable hints when I'm unable to make progress, without which, much more time is expected for finishing this research. My appreciation also attributes to his advices in giving public presentation as well as writing paper and this thesis.

I also should greatly appreciate Lei Yue. With her help, much technique problems during computer simulation were easily solved. The discussion with her also improved my understanding of simulation details as well as fundamental theories behind the simulation.

Dr. Xiaoyang Liu was a constant source of help to me. His help is a constant source for me to solve simulation problems.

Table of Contents

Chapter 1 Introduction	1
Chapter 2 Literature Review	8
2.1 Grain Boundaries.....	8
2.1.1 Definition	8
2.1.2 Description of Grain Boundaries.....	8
2.1.3 Grain Boundary Structure.....	11
2.1.4 Grain Boundary Energy.....	14
2.2 Grain Boundary Migration	16
2.2.1 Theoretical Background of Grain Boundary Migration	16
2.3 Experimentally Determine Grain Boundary Mobility.....	19
2.3.1 Applied Driving Force.....	20
2.3.2 Polycrystal Methods for Mobility Analysis.....	22
2.3.3 Bicrystal Methods for Mobility Analysis	23
2.3.4 Conclusions Draw from Experiments	26
2.4 Using Computer Simulations to Determine Grain Boundary Mobility.....	28
2.5 Grain Boundary Migration Mechanism.....	32
2.5.1 Reason for Study Grain Boundary Migration Mechanism	32
2.5.2 Previous Grain Boundary Migration Models	33
2.6 The Goal of This Thesis	37
Chapter 3 Simulation Methodology	38

3.1 Fundamental Principle of MD Simulation	39
3.2 Temperature Control.....	43
3.3 Simulation Initialization.....	45
3.4 EAM Potential.....	45
Chapter 4 Twist Grain Boundary Migration Mechanism.....	47
4.1 Simulation Geometry	48
4.2 Applied Driving Force.....	50
4.3 Grain Boundary Migration Velocity.....	55
4.4 Statistical Measures for Characterizing Atomic Motions during Migration.....	55
4.5 Simulation Results.....	58
4.5.1 Grain Boundary Mobility	58
4.5.2 Grain Boundary Kinetics.....	61
4.5.3 Single Atomic Motions.....	63
4.5.4 String-like Cooperative Motions	74
4.5.5 String Motion and Shuffling Motion in Stationary Boundaries.....	83
4.6 Simulation Result Discussions	86
4.7 Twist Boundary Migration Mechanism Study Conclusions	91
Chapter 5 Conclusions and Future Work	94
Bibliography.....	95

List of Tables

4.1 Data for calculating driving force at 1300K for $\Sigma 5$ [001] twist boundary.....	59
4.2 Obtained mobility data at 1300K for $\Sigma 5$ [001] twist boundary	59

List of Figures

2.1 Determine two dimensional grain boundaries via two angles: misorientation θ and inclination α [2].	9
2.2 Illustration of (a) tilt grain boundary; (b) twist grain boundary.[2]	10
2.3 Illustration of low angle and high angle grain boundaries [3]	11
2.4 Describing a symmetric tilt grain boundary with misorientation θ via a series of edge dislocations [4].	12
2.5 Schematic illustration of (a) low angle asymmetric tilt boundary (b) low angle twist boundary [4]	12
2.6 Illustration of coincide site lattice formation in a $\langle 001 \rangle$ tilt grain boundary.	14
2.7 Grain boundary energy versus misorientation of $\langle 110 \rangle$ symmetric tilt boundary in Al[8].	16
2.8 Free energy variance for a single atom's migration from grain 1(blue online) to the grain 2(red online).	17
2.9 (a) Bicrystal configuration of the system (b) Orientation to the field	23
2.10 Illustration of bicrystal geometry of (a) wedge technique; (b) reserved-capillary technique; (c) constant driving force technique(quarter loop) and (d) constant driving force technique(half loop technique).[2]	25
4.1 Schematic diagram of the simulation cell. Grain 1 is the lower grain with crystal orientation $[100]$, $[010]$ and $[001]$ in the X -, Y - and Z - directions. Grain 2 is the upper grain rotated about the $[001]$ axis by a misorientation angle θ . The simulation cell is periodic in the X - and Y -directions and the top and bottom surfaces are free.	49

4.2 Illumination of deviation from linear elasticity. Brown area indicates the elastic energy obtained from measurement (non-linear elasticity) while the purple zone represents energy difference between linear elasticity estimation and measurement. Red stars is the measured stress when apply selected strain.....	53
4.3 Obtained elastic energy difference (the green zone) between the two grains.....	54
4.4 Illumination of driving force difference between linear elasticity estimation and measured driving force.....	54
4.5 Linear fit of the grain boundary position versus time	55
4.6 Collective string motions observed in a tilt grain boundary. Red atoms either belong to upper or lower grain while series of colorful atoms indicate observed string motions. [64] ...	56
4.7 Logarithm of grain boundary mobility versus inverse temperature for $\Sigma 5$, $\Sigma 13$ and general twist boundaries. The inset shows logarithm of the pre-exponential factor as a function of the activation energy.....	58
4.8 Kinetics of the three selected twist boundary at 900K.....	62
4.9 The displacement distribution function G_s at eight different time intervals Δt for $\Sigma 5$ boundary.....	64
4.10 The displacement distribution function G_s at eight different time intervals Δt for $\Sigma 13$ boundary.....	65
4.11 The displacement distribution function G_s at eight different time intervals Δt for general high angle twist boundary.....	66
4.12 Boundary plane view (X - Y) of superimposed atomic positions every 0.2 ps for 1000 time	

intervals for $\Sigma 5$ twist boundary. The atoms are colored according to time, where darkest (red online) and lightest (green online) represent starting and finishing times, respectively. The dashed square indicates the unit cell of the coincidence site lattice and arrows denote the single atomic hopping path.....	68
4.13 Angular distribution function of the atoms with displacement around the peak centered at $r=1.28\text{\AA}$ in Figure 4.9.....	70
4.14 Boundary plane view (X - Y) of superimposed atomic positions every 0.2 ps for 1000 time intervals for $\Sigma 13$ twist boundary. The dashed square indicates the unit cell of the coincidence site lattice and arrows denote the possible single atomic hopping directions.	71
4.15 Angular distribution function of the atoms with displacement around the peak centered at $r=1.52\text{\AA}$ in Figure 4.10.....	72
4.16 Boundary plane view (X - Y) of superimposed atomic positions every 0.2 ps for 1000 time intervals for general high angle twist boundary. The arrows denote the possible single atomic hopping directions.	73
4.17 Angular distribution function of the atoms with displacement around the peak centered $r=r_0$ in Figure 4.11.....	74
4.18 Selection of t^* when string size reaches maximum	75
4.19 Identification of all of the atoms that are members of strings of length greater than three at $\Delta t = t^*$ in $\Sigma 5$ boundary X - Y plane when the grain boundary migrates approximately 10\AA . Different colors represent individual strings and the arrows point to the positions where atoms end.....	76

4.20 collective “short jump” in $\Sigma 5$ boundary X - Y plane at $\Delta t=3$ ps. Atoms are colored by time and the arrows point to the positions where atoms end.....	78
4.21 Identification of all of the atoms that are members of strings of length greater than three at $\Delta t =t^*$ in $\Sigma 13$ boundary X - Y plane when the grain boundary migrates approximately 10\AA . Different colors represent individual strings and the arrows point to the positions where atoms end.....	79
4.22 collective “short jumps” in $\Sigma 13$ boundary X - Y plane at $\Delta t=10$ ps. Atoms are colored by time and the arrows point to the positions where atoms end.....	81
4.23 Identification of all of the atoms that are members of strings of length greater than three at $\Delta t =t^*$ in general boundary X - Y plane when the grain boundary migrates approximately 10\AA . Different colors represent individual strings and the arrows point to the positions where atoms end.....	82
4.24 String-like motions captured in Stationary $\Sigma 5$ [001] twist boundary	83
4.25 String-like motions captured in Stationary $\Sigma 13$ [001] twist boundary	84
4.26 String-like motions captured in Stationary general [001] twist boundary.....	85
4.27 4-atom shuffling motion in stationary $\Sigma 5$ twist boundary	86
4.28 String-length distribution function $P(n)$ for $\Sigma 5$, $\Sigma 13$ and general high angle twist boundary at 900K. The inset shows the correlation between the average string length $\langle n \rangle$ and the activation energy for migration Q for three twist boundaries.....	88

Chapter 1 Introduction

Most solid materials such as metals, ceramics and semiconductors are polycrystalline, where a group of small crystals or grains are separated by grain boundaries (GBs). Grain boundaries are the two-dimensional lattice defects separating two regions of identical crystals with the same structure but different orientations. The thermodynamic and kinetic properties of grain boundaries are distinct from bulk materials and usually grain boundaries are the weakest link in the polycrystalline materials. Therefore, the knowledge of grain boundary properties is essential to understand the overall properties of materials.

The grain boundaries network forms material microstructure, which would influence material properties in many aspects. For instance, yield strength depends on the average grain size and creep resistance is determined by the diffusion along grain boundaries. All of these suggest that grain boundaries play a key role in determining material function and structural integrity.

Furthermore, microstructural parameters such as grain size and texture are determined by grain boundary migration. Average grain size directly influences material response to plastic deformation. The smaller the grain size, the higher the material yield strength will be. This crystal size-strength relationship is described by the Hall-Petch relationship:

$$\sigma_y = \sigma_0 + \frac{k}{\sqrt{d}}, \quad (1.1)$$

where σ_y is the material's yield strength, d is the average grain size, k and σ_0 are the material constants. Thus, grain size is considered as a key parameter to be controlled in the optimization process of annealing, hot rolling, forging, extrusion and so on. By the same token, grain boundary migration is essential to material microstructural evolution that takes place during thermo-mechanical processing of polycrystalline materials.

In metallic systems, grain boundaries serve as dislocations barriers, preferred diffusion path and precipitation phase nucleation sites. Creep relies on the diffusions along grain boundary. Increased grain boundary density results in more diffusion paths. Meanwhile, as discussed before, increasing grain boundary density by reducing grain size will increase the difficulty of dislocation movements.

In addition, polycrystalline materials are widely involved in various kinds of electronic applications. Compared to single crystal materials, polycrystalline materials are easier to manufacture and cheaper. Grain boundaries in polycrystalline materials are able to, significantly, influence metal electrical properties. For instance, the higher the grain boundary density is, the lower the electrical conductivity will be. This is because the charge carriers in material would be scattered by grain boundaries and increased grain boundary density would greatly reduce the mobility of charge carriers, therefore decreasing electrical conductivity.

Owing to above reasons, many researchers carried out investigations with respect to grain boundary structure and properties. However, it is an arduous task to experimentally explore the nature of grain boundary structure and properties. The difficulties lie in several aspects.

Firstly, in order to well define a grain boundary, five variables are required: three Euler angles to determine the unit vector of rotation axis and the angle of grain rotation and the other two angles to denote the position of grain boundary or specify the vector normal of the grain boundary plane. It is difficult to precisely control the five variables experimentally.

Secondly, impurities may greatly affect grain boundary properties and migration. Impurity free metals are beyond our capability to produce. Even in highly pure metals, the small amount of impurity would tend to segregate at grain boundaries. Impurity will drag the motion of grain boundary, decreasing boundary mobility and consequently, the grain boundary migration mechanism will be altered. Unfortunately, such influences due to the presence of impurities are unavoidable in experimental studies. Therefore, it is hard to study intrinsic boundary properties experimentally.

Last but not the least, the relationship between gain boundary structure and fundamental grain boundary migration mechanism has not been illuminated. Observable grain boundary migration will only take place at relatively high temperature. However, high-resolution observations of grain boundary migration

dynamic process at high temperature are quite complicated. Current high-resolution grain boundary observation equipments are only able to inspect static image of grain boundary configuration.

The motivation of this research is to explore the relationship between grain boundary structures and grain boundary migration mechanisms for twist grain boundaries. In order to avoid conventional experimental limitations, an easier alternative approach – atomistic simulations is used. Particularly, molecular dynamics (MD) simulation is applied. The reasons for selecting this approach are as follows:

- 1) The five parameters in defining a grain boundary can be easily controlled using computer simulations.
- 2) The only input for simulation is the potential that describe the inter-atomic interaction between atoms for metals.
- 3) Through computer simulation, an impurity free bicrystal configuration system can be easily achieved.
- 4) Grain boundary migration experimental parameters, i.e. temperature, stress and etc. can be controlled with ease.
- 5) Related grain boundary thermodynamics and kinetics properties can be extracted from simulation results.
- 6) Simulation enables us to investigate grain boundary migration at a small spatial scale (sub-atomic) and time scale (picoseconds). Characteristic

atomic motions can be identified through detail analysis of simulation data.

7) Compared to experiments, simulation has a much lower cost

In sum, MD simulation is an effective and easy to control method in investigating grain boundary properties and grain boundary migration mechanism with satisfactory spatial and temporal resolution. The details of MD simulation application will be presented in latter part of this thesis.

Nevertheless, limitations of MD simulations do exist. One of the major limitations of MD simulation lies with its time and length scales. In order to capture the trajectory of all atoms in a simulation system, time resolution should be as small as 10^{-14} seconds (smaller than the Debye frequency). In addition, simulation for a system involving several hundred thousands of atoms via several state-of-the-art CPUs should take no less than several days. Therefore, simulations are usually carried out, at maximum, on the order of 10 nanoseconds and simulation systems normally contain hundreds of thousands of atoms. On the other hand, real experiments for grain boundary migration usually take seconds while grain boundary migration distance reaches on the order of microns. The discrepancy on time and length scale between simulations and experiments leads to a difficulty in comparison between the two. However, as long as the input inter-atomic potentials are reliable, the results obtained from MD simulations are expected to reproduce the right phenomena in real systems and they will provide

additional insight into these problems.

MD simulation results greatly depend on the employed inter-atomic potential. While atomic interactions can, theoretically, be described using fully quantum mechanical techniques, calculation via quantum mechanics method requires extraordinary large computational resources and time which makes this method unrealistic for even several hundreds of atoms. As a result, like many other researchers, we employed empirical potential as an alternative, where the inter-atomic potential is described by functions and the coefficients of such functions are fitted by lattice parameter, elastic constants, cohesive energy, vacancy formation energy and etc. Given that no empirical potentials can absolutely reproduce the real inter-atomic actions, simulation results are sensitive to the choice of potentials. On the other hand, well-parameterized potentials could yield reliable simulation results for specific materials properties. Rather than focusing the accuracy of a single property under specific condition, empirical interatomic potentials emphasize on trends that are insensitive to details of the potential. Details of potential selection will be presented in the latter part of the thesis.

Chapter 2 of this thesis will present some of the earlier research as a literature review. In chapter 2, background on grain boundary structure, previous theoretical models, experimental and simulation methods related to grain boundary migration mechanism will be briefly introduced. In Chapter 3, I mainly introduce the

statistical measures for characterizing atomic motions. Meanwhile, molecular dynamics simulation details such as elastic driving force, temperature control, periodical boundary conditions and selected inter-atomic potentials will be discussed. In Chapter 4, I investigated the atomistic migration mechanisms of a series of twist grain boundaries. The activation energies for grain boundary migration in selected twist grain boundaries are determined. Statistical measures are used to characterize the atomic motions that occur during grain boundary migration. The analysis shows that two types of cooperative atomic motions exist depending on grain boundary local symmetry and different single atom jump patterns can be identified for various grain boundaries. Atomic migration mechanisms for twist grain boundary will be compared among different types of grain boundaries in terms of single atom hop and collective atomic motions. Finally a general mechanism for twist grain boundary migration obtained from current simulation results is presented. In Chapter 5, directions for future work in this area and remaining questions will also be discussed.

Chapter 2 Literature Review

This thesis mainly focuses on the identification of the atomistic mechanisms for grain boundaries migration in twist boundaries. At the beginning of the review session, I will present the definition of grain boundary based upon their structural and energy difference. Earlier theoretical research of grain boundary migration is reviewed and followed by experiments and simulations conducted for grain boundary migration mechanism research. Previous tilt and twist grain boundaries migration models are carefully analyzed, whose merits and limitations are both briefly discussed.

2.1 Grain Boundaries

2.1.1 Definition

Grain boundaries are the interfaces separating two grains with the same crystal structure but different orientations. Usually, interfaces separate regions of two phases with different chemical or physical properties [1], e.g., the interface between boiling water and vapor is segregating two phases with same chemical component but different physical states. The unique characters of grain boundary enable us to describe grain boundaries via geometric parameters.

2.1.2 Description of Grain Boundaries

In two-dimensional space, we could define grain boundary by two angles -- misorientation angle θ and inclination angle α . As shown in Figure 2.1,

misorientation θ determines the relative position of two grains while inclination α is responsible for specifying the exact position of grain boundary. Translation vector t indicates the relative displacement of two grains.

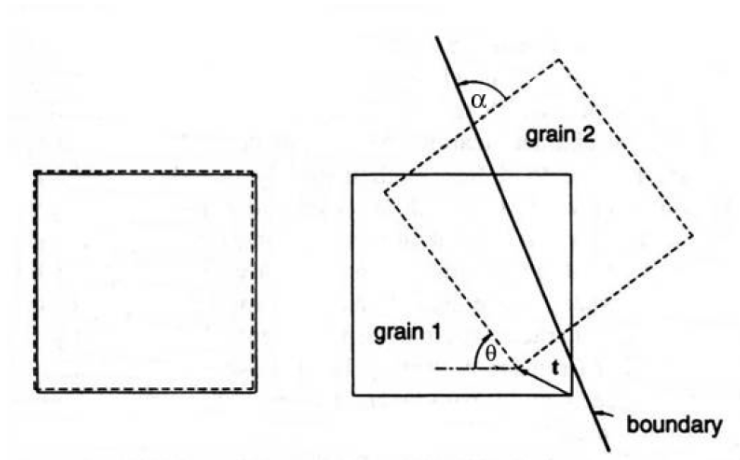


Figure 2.1 Determine two dimensional grain boundaries via two angles: misorientation θ and inclination α [2].

Defining three dimensional grain boundaries is a more complicated task. Misorientation θ is expressed by three Euler angles while inclination α could be expressed by two variables. Consequently, 5 degrees of freedom are required to fully describe a grain boundary. Translation vector t would also introduce three extra freedoms. Fortunately, these three extra freedoms are not readily adjustable. Rather, due to grain boundary energy minimization, they are pre-determined. In this thesis, we intentionally fix other parameters and allow grain boundary property to be a direct function of misorientation angle θ .

Describing grain boundaries through rotation axis and rotation angle allows us to define grain boundaries as tilt boundary, twist boundary or combination of

the two (mixed). A schematic illumination of pure tilt and twist boundary are shown in Figure 2.2, respectively. For tilt boundaries, rotation axis stays within (parallel to) grain boundary plane. Rotation angle is the misorientation between two grains. Dashed lines in Figure 2.2(a) represent a symmetric grain boundary plane while solid lines indicate an asymmetric grain boundary. The angle between the two grain boundaries is determined as grain boundary inclination α . Meanwhile, rotation axes of twist grain boundaries are perpendicular to the grain boundary plane and there is no inclination α , as shown in Figure 2.2(b). As for the mixed grain boundary, the rotation axis is neither parallel nor perpendicular to the grain boundary plane.

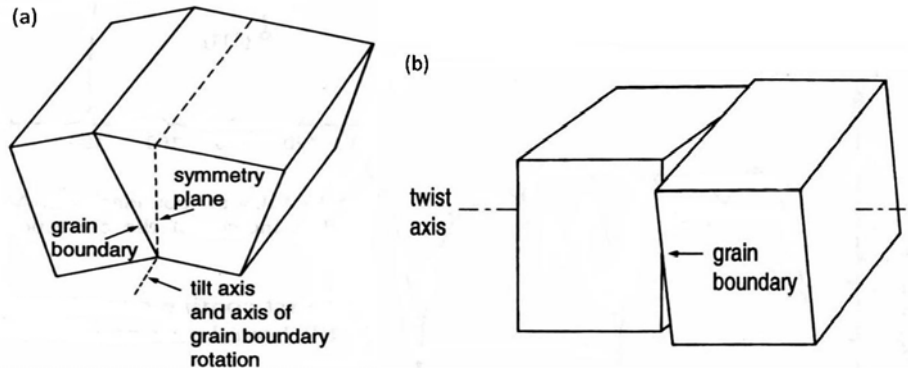


Figure 2.2 Illustration of (a) tilt grain boundary; (b) twist grain boundary.[2]

According to the misorientation angle, we are able to distinguish grain boundaries as high angle and low angle grain boundaries, as indicated by Figure 2.3. While precise division has yet been specified, grain boundaries are often considered as low angle if the misorientation angle $\theta < 15^\circ$.

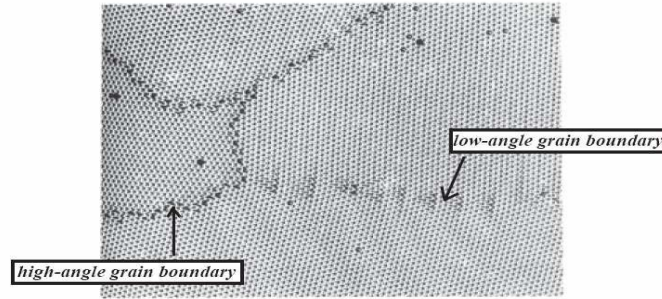


Figure 2.3 Illustration of low angle and high angle grain boundaries [3]

2.1.3 Grain Boundary Structure

Low angle grain boundaries could be described using dislocation model. Figure 2.4 indicates the formation of a symmetric tilt grain boundary via a series of edge dislocations. In this figure, two grains are rotated to each other by $\theta/2$ around the tilt axis, which is perpendicular to the paper. Then, the overall misorientation is θ . As shown in Figure 2.4(b), we treat the steps in grain boundary as arrays of edge dislocations. Distance between each edge dislocation d could be expressed as:

$$\frac{b}{d} = 2 \sin\left(\frac{\theta}{2}\right) \approx \theta, \quad (2.1)$$

where b is the magnitude of the dislocation's Burgers vector. From equation 2.1, we would be able to see that while the rotation angle θ increases, the distance between two edge dislocations d would decrease. When misorientation angle is larger than 15° , dislocation cores tend to overlap and the dislocation model would turn invalid. Hence, 15° is selected as a reasonable transition angle between high and low grain boundaries.

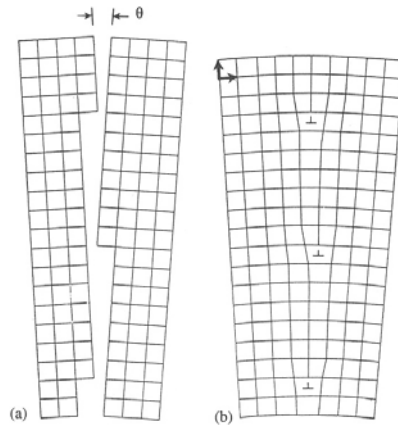


Figure 2.4 Describing a symmetric tilt grain boundary with misorientation θ via a series of edge dislocations [4].

For describing a low angle asymmetric tilt grain boundary, two sets of non-parallel edge dislocations are needed, details shown in Figure 2.5(a). As for describing a twist boundary, at least two sets of screw dislocation are required, illuminated in Figure 2.4(b). Describing a mixed low angle grain boundary with both tilt and twist components will demand at least three Burgers Vectors.

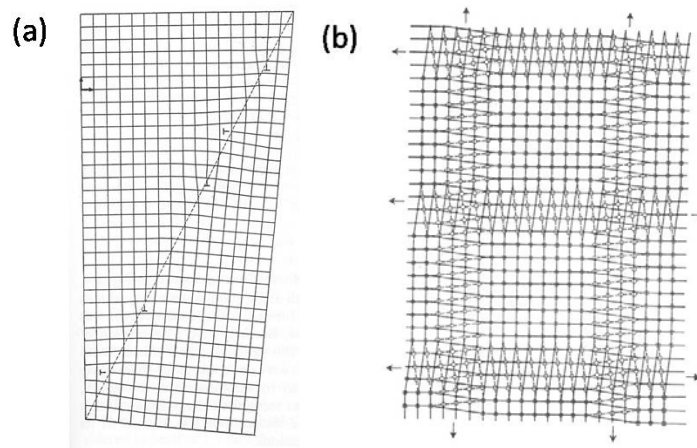


Figure 2.5 Schematic illustration of (a) low angle asymmetric tilt boundary (b) low angle twist boundary [4]

As discussed before, dislocation cores would overlap if rotation angle is

larger than 15° , and the dislocation model is incapable to describe grain boundary structures. Meanwhile, the properties of high angle grain boundaries are essential in determining material properties. Despite the fact that no theories are effective in fully predicting high angle grain boundaries structures, some of the models originated from previous experiments and simulations have certain validity in describing a limited set of specific high angle grain boundaries. For instance, Sutton and Vitek [5] proposed a structural unit model, treating high angle grain boundaries as a series of finite set of atomic units. Pond and Smith employed the secondary grain boundary dislocation model for describing certain high angle grain boundaries [6] .

A very important concept, coincidence site lattice (CSL), should be clarified for exploring grain boundary structure. For constructing CSL, we should first employ two crystals with infinite extent. Then select rotation axis which, at least, should pass one atomic site of each crystal. Rotate one of the crystals to make some of the atoms from both crystals overlap with each other. Finally, the overlapped atomic sites are named as coincide site lattice. The final configuration of CSL is shown in Figure 2.6. Generally, there will be no CSL in grain boundaries. Only when the misorientation reaches specific values can we obtain this unique structure. These special misorientation angles are named as Σ angles. Determination of Σ value follows equation:

$$\Sigma = \frac{\text{elementary CSL cell volume}}{\text{elementary crystal lattice volume}}, \quad (2.2)$$

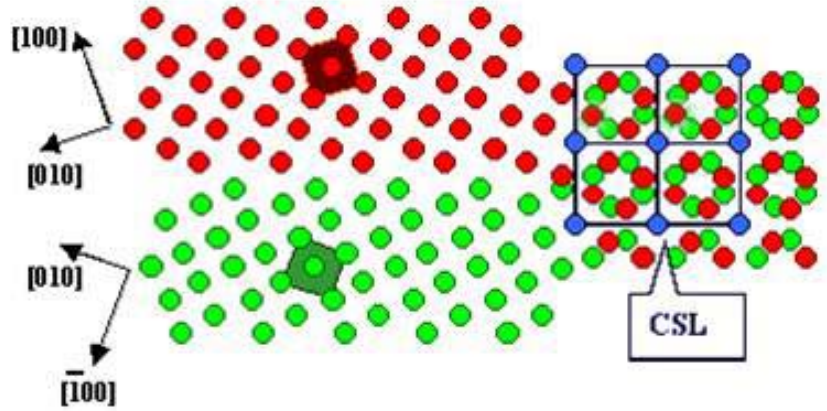


Figure 2.6 Illustration of coincide site lattice formation in a $\langle 001 \rangle$ tilt grain boundary.

Mathematically, all Σ values are odd integers. The smaller the Σ value, the higher the symmetry (orderliness) grain boundary has. In the previous experiments and simulations [7, 8], some of low Σ grain boundaries are found to be special, i.e., low grain boundary energy, high grain boundary mobility and so forth. Despite not all low Σ grain boundaries are special, many of them are unique. That's the reason for focusing on such grain boundaries in this study.

2.1.4 Grain Boundary Energy

Grain boundary energy γ is determined by the excess free energy of the atoms located in grain boundary region. γ is an intrinsic thermodynamic property which can be used to derive all other thermodynamic properties of grain boundary. By definition, grain boundary energy is the energy difference between a bicrystal with a flat grain boundary plane and a single crystal under the same conditions.

Then, the excess free energy is divided by the area of the grain boundary to obtain γ .

The energy of a low-angle grain boundary could be expressed using Read-Shockley dislocation model, i.e., γ is a function of misorientation, θ . For the simple tilt boundaries, where grain boundary is made up of dislocations with Burgers vector b and spacing d , grain boundary energy could be expressed as follows:

$$\gamma_s = \gamma_0 \theta (A - \ln \theta), \quad (2.3)$$

where $\theta = b/d$, $\gamma_0 = Gb/4\pi(1-\nu)$, and $A = 1 + \ln(b/2\pi r_0)$. G represents shear modulus, ν is the poisson's ratio and r_0 is the dislocation core radius. Thus, grain boundary energy becomes a function of grain boundary misorientation. Estimation from this equation perfectly matches the experimental results.[9]

Since high-angle grain boundaries are unable to be described using Read-Shockley model, the mathematical expression of high angle grain boundary energy becomes more complicated. While theories predict that grain boundary energy will be minimum for ideal CSL high angle grain boundaries, experimental results show certain deviations, as indicated by Figure 2.7. The figure shows misorientation dependence of grain boundary free energy for $\langle 110 \rangle$ symmetric tilt boundary in Al [8]. Despite boundaries at misorientations $\Sigma 3(111)$ and $\Sigma 11(113)$ represent the cusps with lowest grain boundary energy, low Σ boundaries, e.g., $\Sigma 9(114)$ and $\Sigma 3(112)$, on the other hand, have high energy. Even not all low Σ

grain boundaries are special, they are still worth investigation. In chapter 4, two low Σ grain boundaries ($\Sigma 5$ and $\Sigma 13$) as well as a general high angle twist boundary will be selected for characterizing twist boundary migration mechanism. So far, no general useful model could predict grain boundary energy dependence on the five variables.

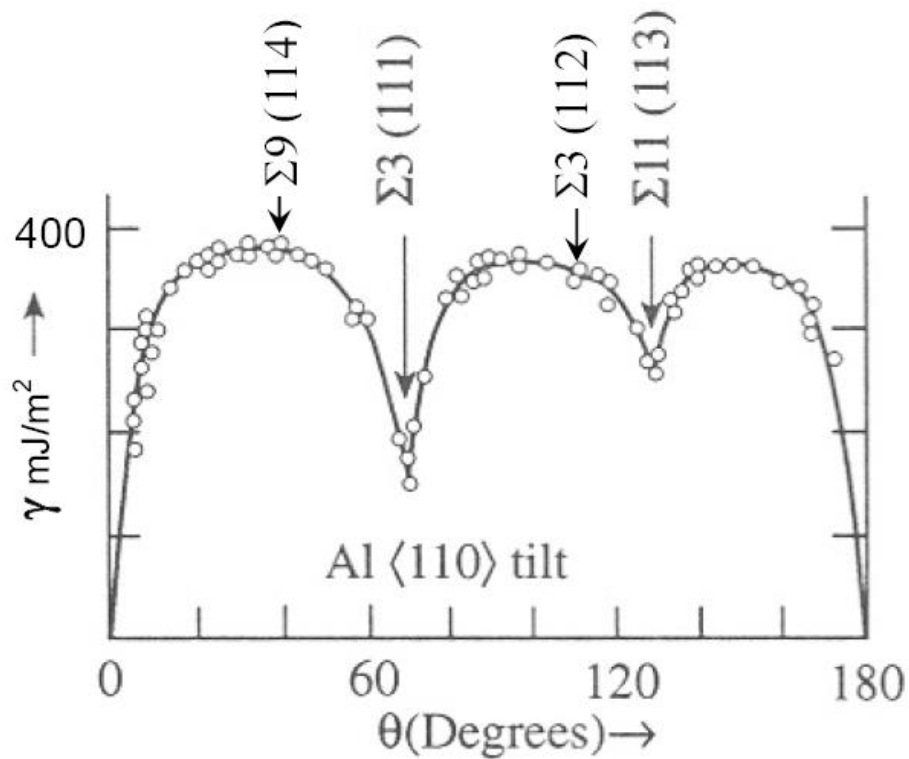


Figure 2.7 Grain boundary energy versus misorientation of $\langle 110 \rangle$ symmetric tilt boundary in Al[8]

2.2 Grain Boundary Migration

2.2.1 Theoretical Background of Grain Boundary Migration

Grain boundary migration is accomplished by reducing the total free energy of the system. Also, grain boundary at the equilibrium state would fluctuate due to

the entropic effects. Generally, external strains, magnetic field , capillary are applied as the driving force for grain boundary migration.

The dependence of grain boundary migration rates on external driving force is illuminated by grain boundary migration mechanism. Reaction rate theory was employed to simply analyze the kinetic process of grain boundary migration [10]. According to this theory, grain boundary migration is treated as an accomplishment of a series of single atomic hopping. The free energy dependence on migrating distance of a single atom hopping is shown in Figure 2.8, where the energy profile of a single atom's migration from grain 1 to grain 2 is illustrated.

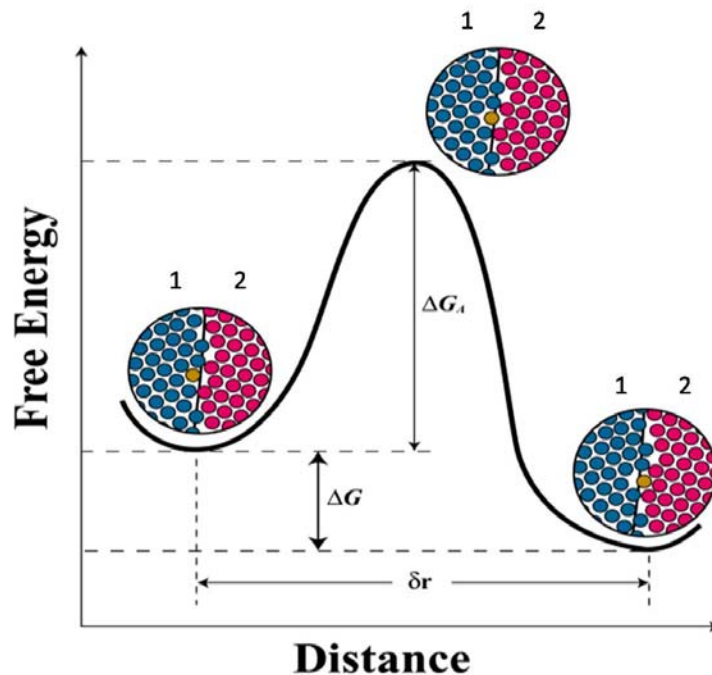


Figure 2.8 Free energy variance for a single atom's migration from grain 1 (blue online) to the grain 2 (red online).

Fullfilling the process of hopping from grain 1 to grain 2 requires the atom to

overcome an energy barrier (ΔG_A). The overall energy difference in this process is ΔG , which is the driving force. Of course, some of the atoms could jump backward from grain 2 to grain 1 as long as they could overcome the energy barrier: $\Delta G + \Delta G_A$. In general, there will be less atoms jump backward due to the necessity of larger energy. Effective flux of atoms migrating from grain 1 to grain 2 could be determined as $A_2 n_1 v_1 \exp(-\Delta G_A / k_B T)$, where n_1 is the number of atoms per unit area in grain 1 that can jump to grain 2, v_1 is the jumping frequency. A_2 is the possibility for atoms to remain in grain 2 when they jump from grain 1 and ΔG_A is the activation energy for a single atom jump. By the same token, the effective flux of atoms migrating from grain 2 to grain 1 could be expressed as $A_1 n_2 v_2 \exp(-(\Delta G_A + \Delta G) / k_B T)$. In equilibrium, $\Delta G = 0$. The flux from grain 1 to grain 2 will be zero. Then, $A_1 n_2 v_2 = A_2 n_1 v_1$. When $\Delta G \neq 0$, the net flux from grain 1 to grain 2 could be expressed as:

$$J_{net} = A_2 n_1 v_1 \exp\left(-\frac{\Delta G_A}{k_B T}\right) \left(1 - \exp\left(-\frac{\Delta G}{k_B T}\right)\right), \quad (2.4)$$

Grain boundary migration rate is obtained by multiple net flux and atomic volume. When ΔG is much smaller compared to $k_B T$, we could expand the exponential $\exp(-\Delta G / k_B T) \approx 1 - \Delta G / k_B T$ and migration rate could be expressed as:

$$v = J_{net} \Omega = \frac{A_2 n_1 v_1 \Omega^2}{k_B T} \exp\left(-\frac{\Delta G_A}{k_B T}\right) \frac{\Delta G}{\Omega}, \quad (2.5)$$

From this equation, we could observe that the migration rate is proportional to the driving force per unit area $\Delta G / \Omega$. Also, we could treat

$\frac{A_2 n_1 v_1 \Omega^2}{k_B T} \exp\left(-\frac{\Delta G_A}{k_B T}\right)$ as a variable M , grain boundary mobility. Then equation

2.5 becomes:

$$v = MP, \quad (2.6)$$

where P represents the driving force and grain boundary mobility could be expressed as:

$$M = \frac{A_2 n_1 v_1 \Omega^2}{k_B T} \exp\left(-\frac{\Delta G_A}{k_B T}\right) = \frac{A_2 n_1 v_1 \Omega^2}{k_B T} \exp\left(\frac{\Delta S_A}{k_B}\right) \exp\left(\frac{-\Delta H_A}{k_B T}\right), \quad (2.7)$$

or

$$M = M_0 \exp\left(-\frac{\Delta H_A}{k_B T}\right), \quad (2.8)$$

where M_0 is the pre-exponential factor and ΔH_A is the activation enthalpy for grain boundary migration.

As shown in equation 2.8, grain boundary mobility is an Arrhenius function of temperature. The linear relationship between grain boundary mobility and driving force is confirmed by several experiments [11, 12] and simulations [13-15].

2.3 Experimentally Determine Grain Boundary Mobility

In this section, experimental geometries and the applied driving force for determining grain boundary mobility are presented. Some of the strategies are utilized in our computer simulations. Major conclusions draw from experiments will also be reviewed.

2.3.1 Applied Driving Force

Based upon equation 2.6, $V=MP$, driving force should be measured before we could extract mobility data. The driving force has the dimension of energy per unit volume, equals the force applied on unit grain boundary area or pressure. Source of driving force could be a gradient of temperature, pressure, dislocation density, magnetic field, etc. Generally, physical anisotropy and capillarity are the most widely utilized driving force.

Capillarity is mainly employed for driving curvature grain boundary migration. Curvature is a geometric variable with the units of reciprocal length. Grain boundary curvature could be described in terms of average grain size. In general, the driving force originated from capillary difference on both sides of the boundary could be expressed as follows:

$$P = \gamma / \alpha, \quad (2.9)$$

where P is the driving force, γ is the grain boundary energy and α represents the curvature radius.

Anisotropy in any physical property, e.g., elastic constants and magnetic susceptibility, could be employed to drive flat grain boundary migration. Mullins [16] was the first to employ magnetic anisotropy as a driving force for grain boundary migration. The driving force resulted from magnetic susceptibilities difference is given by [2]:

$$P = g_{m1} - g_{m2} = \frac{\mu_0 H^2}{2} (\chi_1 - \chi_2), \quad (2.10)$$

where χ_1 and χ_2 are the magnetic susceptibilities of grain 1 and grain 2, respectively, parallel to magnetic field H . When applying magnetic field, the driving force is the magnetic susceptibility difference between two crystals and the driving force could be readily adjusted by altering the strength of applied magnetic field. The disadvantage of such driving force is that only a few materials have large enough anisotropy in magnetic susceptibility.

On the other hand, almost all materials are elastically anisotropic. If we apply an appropriate elastic strain on both crystals, there will be large enough elastic free energy difference between the two, serving as a driving force for grain boundary migration. Let us consider a bicrystal tilt grain boundary configuration with misorientation θ , where the upper grain rotated for the misorientation angle θ while the lower grain maintained unrotated. The X -, Y - and Z - coordinates of the system coincides with lower grain's crystallographic orientations i.e., [100], [010] and [001], respectively. Biaxial strains were applied on the X - and Y - axis of the system while the stresses associate with Z - axis are kept as zero. Thus, the elastic driving force could be expressed as:

$$P = F_1 - F_2 = \frac{(C_{11} - C_{12})(C_{11} + 2C_{12})^2 C_a \sin^2(2\theta)}{C_{11}[4C_{11}(C_{11} - C_{12} + C_a) - (C_{11} + C_{12})C_a(1 - \cos(4\theta))]} \varepsilon^2, \quad (2.11)$$

where $C_a = 2C_{44} - C_{11} + C_{12}$ is the measure of elastic anisotropy and ε is external applied strain. Details could be found in [17].

2.3.2 Polycrystal Methods for Mobility Analysis

Polycrystal methods is based upon the idea that grain boundary mobility data could be extracted from temporal evolution of grain size under the process of grain growth or recrystallization in polycrystalline materials. Despite this method have certain validity for some specific situations, they fail in obtaining grain boundary migration properties since grain boundary mobility was averaged over many different types of grain boundaries. Polycrystal methods could be expressed as follows:

$$\frac{d\bar{R}}{dt} = \frac{C_1 \overline{M(\gamma + \gamma'')}}{\bar{R}}, \quad (2.12)$$

where \bar{R} represents the average grain size. C_1 is a constant. $\overline{M(\gamma + \gamma'')}$ is the averaged reduced grain boundary mobility. γ is the grain boundary energy per unit area and γ'' is its second derivative with respect to boundary inclination.

Owing to the fact that polycrystal methods could only provide average reduced mobility data, relationship between mobility and grain boundary structure as well as the influence of temperature, pressure and etc. on mobility for specific grain boundary are unable to access.

2.3.3 Bicrystal Methods for Mobility Analysis

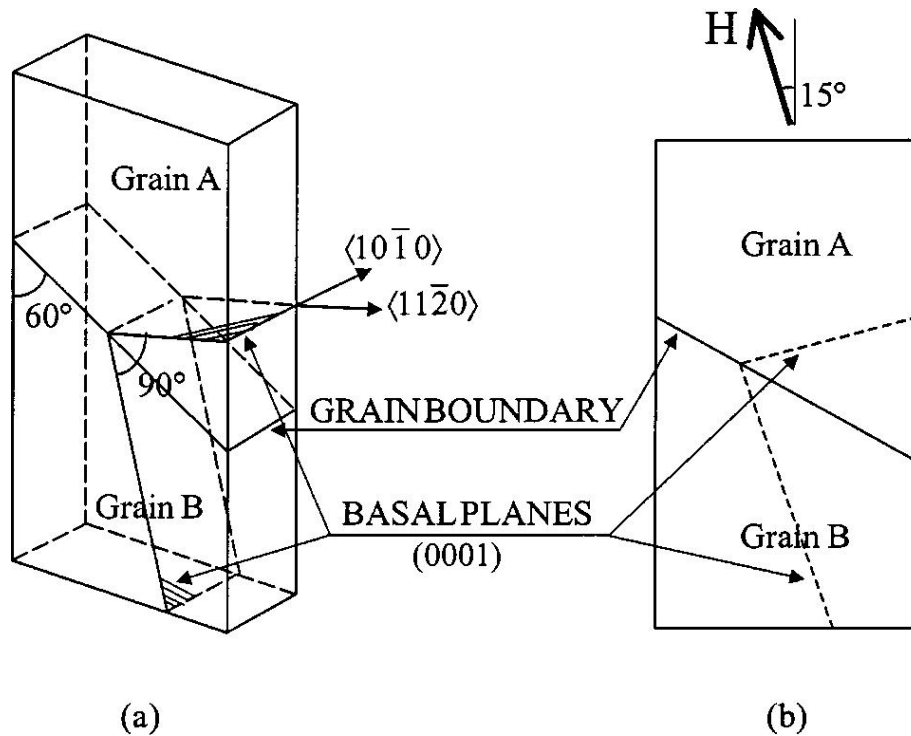


Figure 2.9 (a) Bicrystal configuration of the system (b) Orientation to the field

Two major types of bicrystal geometries were employed for mobility study. One is the flat boundary geometry while applying external elastic strains or magnetic field as driving force. Flat boundary bicrystal structure would be employed in building simulation configuration of this thesis, details of which will be presented later. One example of using bicrystal flat boundary configuration for migration mobility analysis driven by magnetic field is conducted by Sheikh-Ali et al [18]. Configuration of the system as well as the orientation to the magnetic field is indicated in Figure 2.9. Following equation $M = V/P$, absolute boundary mobility was obtained to be about $5.1 \times 10^{-9} m^4 / Js$ at 633K. Winning [19] also conducted experiments with bicrystal structure for migration mobility analysis

driven by external shear stresses. Grain boundary migration velocity was measured by in-situ X-ray diffraction. Strain level influences on activation enthalpy as well as grain boundary mobility's temperature dependence were determined.

The other type is the curved grain boundary geometry with capillary driving force. The advantage of utilizing capillary driving force is that grain boundary surface tension only slightly depends on temperature. Thus, capillary driving force could maintain constant under a wide range of temperatures. In Figure 2.10, three major types of capillary-driven grain boundaries are shown. Figure 2.10(a) shows the "wedge" bicrystal techniques [20-22]. The main advantage of such model attributes to a simple relationship between the driving force P and the radius of curvature a , expressed as

$$P = \sigma_b / a \quad (2.13)$$

where σ_b represents grain boundary surface tension. The limitation of such a geometry is that driving force P would vary, increasing when a decreases during grain boundary migration.

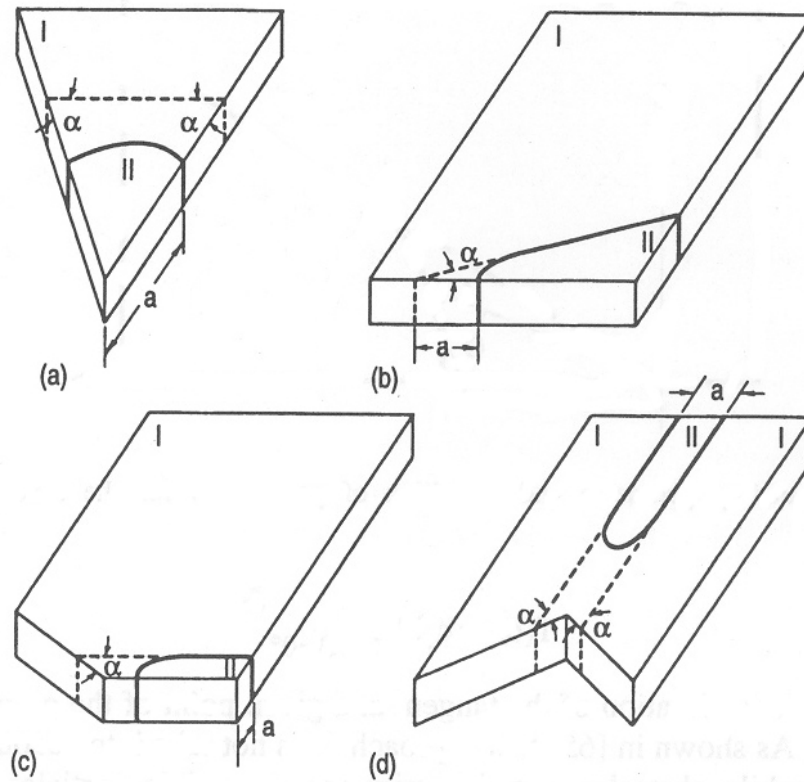


Figure 2.10 Illustration of bicrystal geometry of (a) wedge technique; (b) reserved-capillary technique; (c) constant driving force technique (quarter loop) and (d) constant driving force technique (half loop technique).[2]

Figure 2.10(b) illustrates the reversed-capillary technique, proposed by Sun and Bauer [23, 24]. Such geometry has several advantages. First, it is relatively easy to prepare experimental sample. Second, driving force could be readily altered by changing the angle α . Third, large driving force could be obtained, despite only in the beginning of the experiment. The limitation of such geometry is that driving force are varying and grain boundary migration never reaches steady-state.

In order to reach steady-state grain boundary migration, constant driving

force techniques were developed by Aristov [25] and indicated by Figure 2.10(c) and Figure 2.10(d). Since, grain shape remained unchanged during migration, the driving force is held constant.

2.3.4 Conclusions Draw from Experiments

(1) Most grain boundary migration experiments show a linear dependence between migration velocity and driving force, as indicated by equation 2.6. However, bicrystal experiments of Al via “wedge technique” conducted by Rath and Hu [note 4] found that grain boundary velocity is not correlated with driving force, rather it follows a relationship:

$$V \propto P^n, \quad (2.14)$$

where n ranges from 2 to 12. Rath and Hu attributed this non-linear dependence to the effects of impurity while Gottstein and Shvindlerman suggested it was due to thermal grooving and groove dragging.[26]

(2) Grain boundary migration mobility and temperature follows an Arrhenius relationship, indicated by Equation 2.8. Hence, grain boundary migration is determined as a thermal activated process. Further, from Arrhenius relationship between mobility and temperature, activation enthalpy could also be yielded.

(3) How grain boundary migration and grain boundary diffusion correlated is unanswered. The activation energy for grain growth was found similar to grain boundary self-diffusion activation energy by Cole et al [27] during the investigation of the early stages of the isothermal austenizing in steel. Further,

Sun and Bauer [23] confirmed that activation energy for high angle grain boundary migration and self-diffusion are comparable while studying tilt grain boundary migration in NaCl. However, while investigating the effect of applied pressure on grain boundary migration in Al, Molodov [28] discovered that the activation volume for $\langle 110 \rangle$ tilt boundary in Al was four times larger than single atomic volume. Hence, atomic motions during grain boundary migration in $\langle 110 \rangle$ tilt boundary would be cooperative rather than single atom's hopping -- which is related to grain boundary self-diffusion.

(4) Grain boundary migration is sensitive to the presence of impurities. Aust and Rutter [29] conducted experiments with respect to grain boundary migration in dilute lead-tin alloy. According to the experimental data, grain boundary migration was found sensitive to the content of tin (treat as impurity). In fact, the interactions between grain boundaries and impurities are the origin of the drag effects.

(5) Compensation effect. A series of experiments [30-32] confirmed the mobility and temperature follows an Arrhenius relationship and activation energy and natural logarithm of the pre-exponential factor are correlated with each other. Such a correlation is known as the compensation effect. It has been proved valid for low Σ boundaries while their misorientations stay within a certain ranges. Compensation temperature is defined as the temperature where all grain boundaries within such a misorientation range have the same mobility.

Certain features have been determined by experiments for extracting grain boundary mobility data. While most of these features are sensitive to impurities, impurity-free bicrystal experimental configurations is unavailable. Thus, computer simulation is introduced as an effective alternative measure to obtain grain boundary intrinsic mobility data.

2.4 Using Computer Simulations to Determine Grain Boundary Mobility

Computer simulations serves as an effective method in the determination of grain boundary mobility. With the aid of advanced computer hardware, computer simulation enable us to study some aspects of grain boundary migration which are not accessible by conventional experiments. Via computer simulations, grain boundary migration mechanism could be characterized by analyzing the trajectory of all atoms in the system during migration. Nevertheless, computer simulation also have certain limitations. As discussed before, the major disadvantage of computer simulation is the discrepancy in spatial and temporal resolution between simulations and experiments. In addition, simulations are, more or less, inaccurate because of the input for describing atom interactions are not absolutely definite. Hence, we should only treat computer simulation as a supplement to real experiments, serving as an alternative when experiments are unpractical under certain conditions.

The first simulation for obtaining grain boundary migration mobility

employed elastic strain as driving force was carried out by Schonfelder et al. [15]. In this simulation, a flat $\Sigma 29$ twist grain boundary migration was studied. Lennard-Jones potential for copper was employed for describing atomic interactions for copper. The driving force originated from the elastic free energy difference between two grains. Then main findings of the simulations were: (1) grain boundary migration rate and driving force followed a linear relationship while applied strain is up to 4%, thus absolute grain boundary mobility could be determined; (2) Grain boundary migration activation energy was found sufficiently smaller than that of grain boundary diffusion; (3) grain boundary migration mobility follows an Arrhenius relationship with temperature and the activation energy was yielded to be 0.23 eV/atom. While the activation energy for each atom obtained from experiments are much larger than the value extracted in this simulation, it is inappropriate to simply attribute the discrepancy to selected inter-atomic potential.

Further, Upmanyu et al. studied curvature driven tilt grain boundary migration using molecular dynamics simulation [13]. Atomic interaction was described by a Lennard-Jones two-body potential. In this simulation, reduced mobility, $M^* = M(\gamma + \gamma'')$, was extracted. As experiments commonly measure reduced mobility rather than real mobility, this simulation's results could be directly compared with the data obtained from experiments. The activation energy dependence on misorientation obtained from MD simulation was consistent with

that from experiments. However, activation energy, itself, extracted from simulation was smaller than experimental value. This variance could be attributed to the effects of impurities [33, 34]. The limitation of such simulations lies in the difficulty in obtaining the real mobility from extracted reduced mobility data. Moreover, by using curved boundary geometry, it is unable to investigate the dependence of mobility on other parameters, e.g., grain boundary inclination.

The simulations listed above are valid measures to obtain absolute and reduced grain boundary mobility. Meanwhile, activation energy could also be derived. However, activation energy obtained from simulations is sufficiently smaller than those extracted from experiments. Despite we could attribute this discrepancy, in part, to the existence of impurities in experiments, we still need to guarantee the selection of accurate inter-atomic potentials for MD simulations. Both simulations presented above employed the simplistic Lennard-Jones potential.

In order to achieve more accurate simulation results, more realistic inter-atomic potentials are employed in simulations. Zhang et al. conducted curvature driven grain boundary migration in Al [35], employing embedded atom method (EAM) inter-atomic potentials [36]. Migration of a series of $\langle 111 \rangle$ tilt boundaries in aluminum were simulated. Reduced mobilities were obtained and determined to be an Arrhenius function of temperature. Compared with experimental results, obtained mobilities were much higher while lower activation

energies were yielded from simulations.

Janssens et al [37] conducted MD simulations in order to determine mobility of twist flat boundaries with misorientations ranging from 10° to 60° . An artificial crystal-orientation-dependent driving pressure was employed to compute the grain boundary mobility in the fcc Al. Inter-atomic potential was real Aluminum EAM potential and modified for obtaining desired driving force. Rotation axis was selected around [111] crystallographic direction. For a series of investigated symmetric boundaries, grain boundary mobility was found increasing while rotation axis deviating from [111] axis, as expected. However, some unexpected results were observed, e.g., some mixed boundaries of $\Sigma 3$ misorientations have high mobility. Simulation results are consistent with those from experiments. Moreover, simulations added more details, therefore enriching experimental investigations.

Upmanyu et al [38] performed a zero driving force MD simulation, with EAM-Al inter-atomic potential. Absolute interface mobility was obtained by tracking random walk of averaged interface position along interface normal. Simulation results validated and also emphasized predicted impurities' effect. Mobility data obtained by employing Lennard-Jones potential was assumed to underestimate the boundary mobility by at least an order of magnitude. Methodology developed in this simulation provides a successful measure to quantify impurity effect at atomic scale.

2.5 Grain Boundary Migration Mechanism

2.5.1 Reason for Study Grain Boundary Migration Mechanism

Although, we could obtain temperature dependence on grain boundary mobility by employing the reaction rate theory, treating grain boundary migration as a series of non-correlated single atom hopping, many experimental and simulation results [14, 39-43] suggest the existence of cooperative motions between these jumping atoms. For instance, Jhan and Bristowe [42] claimed a 4-atom shuffling motion while studying a curvature driven twist boundary migration, which was experimentally confirmed by Babcock and Balluffi [43]. Zhang et al also reported collective motions[39-41], which they named as string motions, while simulating a series of tilt grain boundaries. Related details will be discussed in later session. All of these discoveries supported the idea that some of the atoms are moving in a cooperative manner. Meanwhile, activation energy for grain boundary migration is found much smaller compared with that for grain boundary diffusion [14, 15, 44]. Thus, grain boundary migration and grain boundary self-diffusion are determined as two unique processes.[14] In sum, reaction rate theory is incapable for describing grain boundary migration details.

Nevertheless, experiments and simulation results, so far, are not good enough for building a more reliable model due, in part, to the complexity of the grain boundary migration process. Furthermore, data with respect to details of atomic movements are not readily accessible by utilizing conventional measures. Thanks

to computational simulations, we are able to track a large number of atomic motions under a satisfactory time and space resolution, monitoring the overall process of grain boundary migration. Now the task becomes how to analyze the vast data collected from computer simulations for yielding grain boundary migration mechanism.

The necessity of building a general grain boundary migration mechanism model lies in the requirement for describing grain boundary motions associated with a large number of different materials and grain boundary bicrystallography. By utilizing atomistic simulations, mechanisms of grain boundary migration could be determined, and, hence, a theory based upon the mechanism could be established for determining some unknown elements, i.e., grain boundary structure. Consequently, this thesis is motivated by investigating several special twist grain boundary migration mechanism in fcc metal Nickel and pave the way for future establishment of a general migration model for twist grain boundaries in variety kinds of materials.

2.5.2 Previous Grain Boundary Migration Models

Many works in the past several decades have been focused on the atomistic mechanisms for grain boundary migration. As discussed in grain boundary energy session, Read and Shockley [9] suggested that for a low angle grain boundary, migration could be described in term of the motion of dislocations. As discussed before, by utilizing such a dislocation model, grain boundary is treated as a series

of edge dislocations for pure tilt grain boundaries while pure twist boundaries are composed of a set of screw dislocation. Grain boundaries migrate via gliding and climbing of the dislocations. Obviously, the limit of the dislocation model is its incapability of describing grain boundary migration for high angle grain boundaries when dislocation cores overlap. Island model, proposed by Mott [45] and improved by Gifkins [46], describes grain boundary migration as a movement of a group of perfect crystalline island that melt from one side of the boundary and solidified on the other side. This island model is hard to justify due to the highly structured nature of the very narrow grain boundaries seen in high resolution electron microscopy [47]. Gleiter[48], however, suggested grain boundary that consisted of terraces, ledges and kinks could migrate by grain boundary atoms detaching from kinks and ledges, propagating on the terraces and adhering to the opposite grain boundary surface. Despite this model do account for grain boundary structure, it is only an idealized form as related parameters are not verified by any experiment or simulation. Further, such model also implies a wide grain boundary structure which is contradict to experimental observations[2]. Pond and Smith [6] schemed grain boundary migration by the motion of the secondary grain boundary dislocation (SGBD) within the Coincidence Site Lattice (CSL). In large angle grain boundaries, the dislocations are found to have smaller Burgers vector compared to that of lattice dislocations. Such dislocations are frequently named as secondary grain boundary dislocations (SGBD) or DSC-

dislocations. The existence of the secondary grain boundary dislocation was verified by and Balluffi [49]. However, the validity of this model is confined to only several high angle Σ grain boundaries. Further, recent experiments [50] have shown that the contribution from the motion of SGBD is negligible. In a whole, none of those models provides a particularly complete description of the atomistic mechanism for describing grain boundary migration.

While grain boundary structures at low temperature can be characterized using modern high-resolution electron microscopy, grain boundary structures and migration at high temperature are hardly accessible via these experimental measurements. As an alternative, atomistic simulation is a perfect approach to explore this problem. Over the last three decades, a number of works have been reported on the identification of the atomistic mechanisms for grain boundary migration using molecular dynamics (MD) simulation. Jhan and Bristowe [42] reported an atomic shuffle mechanism in the study of curvature driven grain boundary migration of a $\Sigma 5$ twist boundary. By observing sequence of snapshots of the grain boundary plane, a series of 4-atom cooperative motions were observed and a propagation of such shuffling was believed to be the mechanism of $\Sigma 5$ twist boundary migration mechanism. This was supported by experimental results from Babcock and Balluffi [43]. Bishop et al. [51] and Cahn et al. [52] investigated the atomistic mechanism for flat grain boundary migration induced by external shear stress. They concluded that grain boundary migration, the

motion perpendicular to the grain boundary plane, was coupled with grain boundary tangential displacement -- the motion parallel to the boundary plane. The rate of such tangential motion is proportional to the migration rate of the interface. Grain boundary migration of a series of $\Sigma 5$ [001] twist boundary driven by elastic strain energy in copper was investigated by Schonfelder et al. [14]. In this study, the authors confirmed that grain boundary migration for low angle twist grain boundaries was assisted by the motion of a network of screw dislocations, while 4-atom collective shuffle mechanism was responsible for the migration of $\Sigma 5$, $\Sigma 17$ and $\Sigma 29$ grain boundaries. However, the migration mechanisms for $\Sigma 13$ and $\Sigma 25$ were hard to identify.

Recently, Zhang and Srolovitz [39] performed MD simulations to identify the atomistic mechanisms for grain boundary migration in a series of $\Sigma 5$ [001] tilt grain boundaries. Two major distinct types of atomic motions were identified during migration -- string-like cooperative motions parallel to the tilt axis and single atom jump across grain boundary plane. These two types of atomic motions were confirmed in a further study [41] using statistical measures such as van Hove correlation function, dynamic entropy and non-Gaussian parameter. In addition, a quantitative measure of the cooperatives motion was developed. More recently, these methods have been used to identify the atomistic mechanisms for general [001] tilt grain boundary [40] and similar conclusions were obtained. These developed statistical measures are used for specifying twist grain boundary

migration mechanism in this thesis.

2.6 The Goal of This Thesis

Obtaining grain boundary mobility value is not the ultimate goal for our study on grain boundary migration. Rather, unambiguous understanding how grain boundary move – the migration mechanism is our destination. The focus of this thesis is to illuminate the atomistic migration mechanisms of several special twist grain boundaries and provide guidelines for generating universal grain boundary migration mechanisms in the future. Although some previous works have been focused on the migration mechanisms for [001] twist grain boundary, many questions associated with the atomic motions during twist grain boundary migration are yet answered. For instance, is there any correlation between individual 4-atom shuffles in $\Sigma 5$ grain boundary? Is the migration mechanism of $\Sigma 5$ twist boundary to be the propagation of reported 4-atom shuffling? What is the atomistic migration mechanism for $\Sigma 13$ grain boundary, which is claimed to be difficult to specify in previous simulations? How does the migration mechanism change when grain boundary changes from a CSL boundary to a non-CSL boundary? To answer these questions, I will use the statistical measures that were previously developed in the study of tilt grain boundaries to investigate the atomic motions that govern grain boundary migration in twist grain boundaries. Details of the simulation as well as statistical measures are presented in Chapter 4.

Chapter 3 Simulation Methodology

In the previous chapters, I presented the advantage of employing molecular dynamics simulation for grain boundary migration study. In this chapter, details of simulation methods, especially the algorithms for integrating Newton's equations, temperature control, simulation configuration construction and the selection of inter-atomic potentials will be discussed.

Through numerical integration of Newton's equations of motion for each atom, MD simulation could obtain thermodynamic, structural and kinetic properties, e.g., yield strength, interfacial energy, diffusivity and etc. Alder and Wainwright first introduced the MD methods in 1950's [53, 54] while studying the dynamics of an assembly of hard spheres. MD simulation for real materials was conducted by Gibson et al [55] in analyzing copper's radiation damage dynamics. Rahman was the first to employ realistic potential while simulating liquid argon [56].

As discussed before, MD simulation is able to perform under the conditions that beyond experiment's capability. For instance, five variables for describing grain boundary crystallography could be readily fixed. In addition, experimental conditions, i.e., temperature, pressure and chemical potentials, are easy to control. Further, with the aid of computer simulation, thermodynamics properties as well as temporal evolution are easily accessible.

One of the major limitation of computer simulation is its discrepancy in spatial and temporal resolution with real experiments. Nevertheless, the application of periodic boundary conditions provides an approach to extend simulation system from a finite small volume to infinitely large. For truly periodic systems, e.g., periodic single crystal, only small simulation system is needed. However, when we deal with systems with defects or calculate kinetic and dynamical quantities, large simulation system is needed. Normally, largest simulation system may contain atoms on the order of 10^9 . Due to the wide-spread interest on nano-scale materials, spatial resolution of real experiment and that of simulation becomes closer. Now, the the discrepancy becomes temporal resolution inconsistency.

In the following section, I will present the fundamental principles of the MD simulation method, employed algorithm and the choice of inter-atomic potentials.

3.1 Fundamental Principle of MD Simulation

Molecular dynamics simulation is based upon Newton's second law:

$$F_i = m_i a_i, \quad (3.1)$$

where F_i , m_i and a_i are the force, mass and acceleration of atom i , respectively. Since the force on each atom is determined from potentials, acceleration of each atom could be calculated. Hence, integration of the equation of each atom yields the trajectories (positions, velocities and accelerations) of each atom as a function of time. Thus, the average values of system properties could be determined. We

only need initial position and velocity of the system as an input for MD simulation.

Force of each atom could be calculated via given inter-atomic potential, shown as follows:

$$F_i = -\nabla_i V_i, \quad (3.2)$$

where V represents inter-atomic potential. Combining equation 3.1 and 3.2 could yield:

$$-\frac{dV}{dr_i} = m_i \frac{d^2 r_i}{dt^2}, \quad (3.3)$$

where r_i represents the i^{th} atom's position.

From equation 3.3, we could see that the most important input for MD simulation is the interatomic potential V . Different materials would have distinct V . While accuracy of potential would directly determine simulation results' reliability, one can use various kinds of potentials ranging from empirical, semi-empirical to full quantum mechanical. Frequently employed potentials for simulation with respect to metals are two-body potentials, treating the overall energy of the system as a sum of atomic pairwise interactions and many-body potentials by summing a larger group of atoms.

Lennard-Jones 6-12 potential is a classical two body potential which could be expressed as follows:

$$V = 4\varepsilon\left(\left(\frac{\sigma}{r}\right)^{12} - \left(\frac{\sigma}{r}\right)^6\right), \quad (3.4)$$

where ε is the depth of the energy well and σ is the interparticle spacing when

pairwise potential equals zero. Lennard-Jones potential could be divided into two parts – an attractive part and a repulsive part. Despite the fact that Lennard-Jones potential is incapable of accurately describing specific material's properties, it does have certain merits. Also, pair-wise potential generally requires less computer sources compared with many-body potentials.

Many body potentials, on the other hand, accounts for interactions between pair-wise atoms. Embedded Atom Method potential [36] is one of the important types of many body potentials, which was employed in the simulations conducted in this thesis. Since EAM potentials include a many-body force term to take the electron density into account, such potentials are widely utilized in simulating metals. EAM potential is constituted by a pair-wise term plus a local electron density term – describing a n-body interaction. Details of EAM potential would be presented later. Generally, many-body potential is capable of describing more accurate atomic interactions while demanding more computing sources.

Given that potential energy is a function of the positions of all atoms within system, it is impractical to integrate Newton's equations of motion. Thus, we resort to numerically solve such set of equations of motions. The algorithm for such numerically solution should acquire following features: (1) energy and momentum of the system should be conservative; (2) computational efficient; (3) the round off errors should be small enough for long time accurate integration. The most basic numerical integration method is Euler method, following

equations:

$$r_i(t + \delta t) = r_i(t) + v_i(t)\delta t, \quad (3.5)$$

and

$$v_i(t + \delta t) = v_i(t) + \left(-\frac{\partial U}{\partial r_i} \cdot \frac{\delta t}{m_i}\right), \quad (3.6)$$

where r_i , v_i respectively represent position and velocity of atom i . t and δt on behalf of a certain timestep and time interval. V is employed force-field and m_i is the atom i 's mass. With already known initial position and velocity of each atom and the inter-atomic potential, positions and velocities at latter time could be calculated in a succession of timesteps. However, such method is not accurate and would not be utilized in our simulations.

One of the most commonly used integration algorithms is the Verlet algorithm [57, 58]. The fundamental idea of such a algorithm is to expand the particle position in the previous and next time step in the Taylor series:

$$r(t + \delta t) = r(t) + v(t)\delta t + \frac{1}{2}a(t)\delta t^2 + \dots, \quad (3.7)$$

and

$$r(t - \delta t) = r(t) - v(t)\delta t + \frac{1}{2}a(t)\delta t^2 + \dots, \quad (3.8)$$

where δt and v are MD simulation timestep and velocity respectively. By combining equation 3.7 and 3.8 we could obtain:

$$r(t + \delta t) \approx 2r(t) - r(t - \delta t) + a(t)\delta t^2, \quad (3.9)$$

With position and acceleration at time t and position at $t-\delta t$, position at $t + \delta t$ could be determined. Error of such algorithm is δt^4 . The advantage of such algorithm attributes to the unnecessary of velocity data for estimating the positions of following timesteps. However, when we need calculate velocity, the accuracy of obtained velocity is only on the order of δt^2 . To increase obtained velocity's accuracy, we could use velocity Verlet algorithm with following form:

$$r(t + \delta t) = r(t) + v(t)\delta t + \frac{1}{2} a(t)\delta t^2, \quad (3.10)$$

and

$$v(t + \delta t) = v(t) + \frac{1}{2}[a(t) + a(t + \delta t)]\delta t, \quad (3.11)$$

Velocity Verlet algorithm has same accuracy level for predicting new atomic positions as Verlet algorithm does. Meanwhile, the accuracy of velocity estimation would be up to δt^4 . Despite such algorithm has more or less numerical errors, the simulation results are reliable in a statistical or ensemble sense.

3.2 Temperature Control

Classical MD simulation of N particles system with volume V corresponds to a microcanonical ensemble (NVE ensemble), i.e., number of atoms, volume of the system and total energy are conserved during simulation. However, in this thesis, we need to perform NVT ensemble (canonical ensemble) where temperature is conserved. Then, we should employ other methods to maintain temperature to be constant.

Variety kinds of means are available for maintaining temperature during MD simulations. The approach we employed is rescaling velocity owing to that velocity and system temperature could be expressed as follows:

$$\left\langle \sum_i \frac{1}{2} m v_i^2 \right\rangle = \frac{3}{2} N k_B T, \quad (3.12)$$

where m is the mass; v_i is the velocity; N is the number of atoms in system; k_B is the Boltzmann constant and T represents the system temperature. We could rescale the velocities at each timestep by a factor of $(T/T_i)^{1/2}$, where T is the desired temperature while T_i is the instantaneous temperature at timestep i .

An alternative approach to maintain constant temperature is to introduce an extended Lagrangian approach in modifying Newton's equation of motion. This method was first introduced by Anderson [59] in performing a constant pressure simulation. Nosé – Hoover thermostat is the classical type of such approach [60, 61]. Employing extended Lagrangian to maintain constant temperature in MD simulation based upon the assumption that the simulation system is in contact with a thermal reservoir which have additional degrees of freedom. Energy exchange between the system and the reservoir is allowed. The total energy of the simulation system plus the thermal reservoir is conserved.

Stochastic approach proposed by Anderson [59] coupled the system with a heat bath to achieve desired system temperature. The coupling to a heat bath is accomplished using stochastic forces on random selected particles. By employing

this method, a random particle is first selected at certain interval. Then, resample the atom's velocity components from Maxwell-Boltzman distribution by colliding with the heat bath particle. Between the interval, system evolves in a microcanonical (NVE) measure and the limiting probability distribution is canonical (NVT). The time between collisions is sampled from a Poisson distribution.

3.3 Simulation Initialization

In the initialization of simulation system, atoms of certain configuration will be inputed. We randomly assign velocity of each atom from a Maxwell distribution to obtain desired temperature. Alternatively, assigning velocities to atoms from a uniform random distribution could also lead to Maxwell temperature distribution. Timestep in MD simulation of this thesis was chosen to be femtosecond, i.e. , 10^{-15} second.

Periodic boundary condition is employed in MD simulation of this thesis. In order to maintain a constant driving force, we constructed free surface on up and bottom part of the simulation configuration. Details of boundary conditions would be presented in latter part of the thesis.

3.4 EAM Potential

The many-body potential employed in MD simulation is the EAM potential. EAM was firstly developed by Daw and Baskes [36]. By employing EAM potential, the energy of the metal is obtained by embedding an atom into the

electron density created by remaining atoms of the system. The potential energy of the system could be expressed as:

$$E = \frac{1}{2} \sum_{i,j(i \neq j)} U_{ij}(r_{ij}) + \sum_i G_i(\rho_i), \quad (3.13)$$

and

$$\rho_i = \sum_{i \neq j} \rho_j^a(r_{ij}), \quad (3.14)$$

where $U_{ij}(r_{ij})$ is pairwise potential between atom ij with separation r_{ij} . $G_i(\rho_i)$ represents the energy required for embedding an atom i into uniform electron density ρ_i , while ρ_i is the spherically averaged atomic electron density at atom site i created by all of the rest atoms in the system. The EAM potential has been proved to be effective in studying grain boundaries in metals, which is the reason why it is selected for MD simulation in this thesis. Exactly, in this thesis, the atomic interactions were described using the Voter-Chen form of the Embedded Atom Method (EAM) potential for Nickel. The selection of nickel in this simulation is due to its large elastic anisotropy. Under the same elastic strain, Ni would have larger driving force compared with other FCC metals, e.g., Al.

Chapter 4 Twist Grain Boundary Migration Mechanism

In this chapter, I will focus on the migration of a series of $\Sigma 5$ [001] twist grain boundaries in Ni. The atomic interactions were described using the Voter-Chen [62] form of the Embedded Atom Method [36] (EAM) potential for Ni. The simulations were performed within a NVT ensemble (Fixed numbers of atoms, volume and temperature). Constant temperatures of 900K, 1000K, 1100K, 1200K, 1300K, 1400K and 1500K were maintained using a rescaling scheme. The melting point of this potential is 1624K [40]. The total number of atoms for $\Sigma 5$, $\Sigma 13$, and general boundaries simulation cell were 128000, 54076 and 92721, respectively. Atomic configurations of the simulation cell were saved every 0.2ps for further study. MD Simulations were performed using large-scale atomic/molecular massively parallel simulator (LAMMPS) [63], developed at Sandia National Laboratory. The purposes are to (1) investigate grain boundary mobility's temperature dependence; (2) characterize rate controlling atomic motions for grain boundary migration of each selected twist boundary; (3) determine the relationship between grain boundary migration mechanism and grain boundary misorientation. In the following sessions, I will describe the applied driving force, simulation geometry, methods for extracting grain boundary mobility data and the statistical measures for identifying grain boundary migration

mechanism. Simulation results were carefully examined and the mechanisms for each investigated twist boundary were specified. A general trend of migration mechanism transition from Σ twist boundaries to non- Σ twist boundary was also yielded.

4.1 Simulation Geometry

In the thesis, I performed three dimensional molecular dynamics simulations of grain boundary migration in a series of [001] twist grain boundaries in fcc nickel. In Particular, a $\theta=36.87^\circ$ $\Sigma 5$ boundary, a $\theta=22.63^\circ$ $\Sigma 13$ boundary and a $\theta=40.23^\circ$ general boundary (non-CSL boundary or $\Sigma=\infty$) were considered. Figure 4.1 shows the schematic of the bicrystal simulation cell with a flat grain boundary. The bicrystal consisted of a lower grain (grain 1) with the crystal orientations [100], [010] and [001] in the X -, Y - and Z -directions, respectively, and an upper grain (grain 2) rotated about the [001] axis by angle θ . The misorientation angle θ was defined as the relative angle between the [010] axis of the upper and lower grains. The grain boundary plane was perpendicular to the Z -axis as the figure indicated. Periodic boundary conditions were applied to the X - and Y - directions while free boundary condition was applied in the Z -direction, resulting two free surfaces on the top and the bottom in the simulation cell.

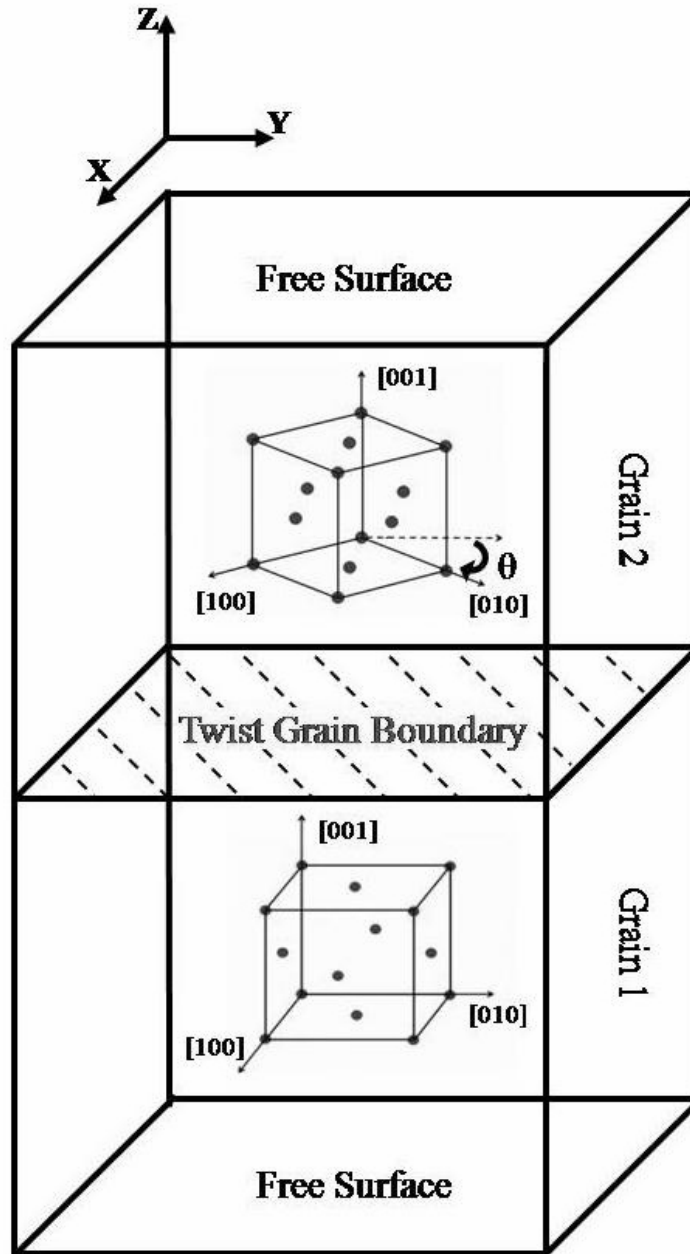


Figure 4.1 Schematic diagram of the simulation cell. Grain 1 is the lower grain with crystal orientation $[100]$, $[010]$ and $[001]$ in the X -, Y - and Z - directions. Grain 2 is the upper grain rotated about the $[001]$ axis by a misorientation angle θ . The simulation cell is periodic in the X - and Y -directions and the top and bottom surfaces are free.

4.2 Applied Driving Force

It is widely accepted that grain boundary migration is a thermally activated process, as discussed in Session 2.21. Based on this, grain boundary migration velocity v can be written as mobility M times driving force P

$$v = MP \quad M = M_0 \exp\left(-\frac{Q}{k_B T}\right), \quad (4.1)$$

where M_0 is the pre-exponential factor, k_B represents the Boltzmann constant and Q is the activation energy for grain boundary migration. In the steady state migration condition grain boundary migration velocity could be obtained by linear fitting the temporal evolution of the average grain boundary position. Consequently, grain boundary mobility can be calculated if the driving force is known.

The driving force employed in this study is the stored elastic strain energy density difference between two grains. Since most crystalline solids are elastically anisotropic as discussed in previous chapters, the driving force can be expressed as,

$$P = \left(F_{elastic}^{Grain2} - F_{elastic}^{Grain1}\right), \quad (4.2)$$

where $F_{elastic} = \frac{1}{2} C_{ijkl} \varepsilon_{ij} \varepsilon_{kl}$ is the elastic strain free energy. The applied strains and stresses are as follows:

$$\varepsilon_{ij} = \begin{pmatrix} \varepsilon_{xx} & 0 & \varepsilon_{xz} \\ 0 & \varepsilon_{yy} & \varepsilon_{yz} \\ \varepsilon_{xz} & \varepsilon_{yz} & \varepsilon_{zz} \end{pmatrix}, \quad (4.3)$$

$$\sigma_{ij} = \begin{pmatrix} \sigma_{xx} & \sigma_{xy} & 0 \\ \sigma_{xy} & \sigma_{yy} & 0 \\ 0 & 0 & 0 \end{pmatrix}, \quad (4.4)$$

Note, we applied ε_{xx} and ε_{yy} in the X - and Y -direction by controlling the periodic boundary conditions and applied zero stress along the Z -direction using free boundary condition (free surfaces). Therefore, the elastic free energy in the lower grain is estimated as:

$$F_{elastic}^{Grain1} = \frac{(C_{11}^2 - C_{12}^2)\varepsilon_{xx}^2 + 2(C_{11} - C_{12})C_{12}\varepsilon_{xx}\varepsilon_{yy} + (C_{11}^2 - C_{12}^2)\varepsilon_{yy}^2}{2C_{11}}, \quad (4.5)$$

The elastic free energy in the upper grain can be also estimated using Hook's law with proper rotation as:

$$F_{elastic}^{Grain2} = \frac{1}{8C_{11}} \left\{ \begin{aligned} & \left[3C_{11}^2 + C_{11}C_{12} - 4C_{12}^2 + 2C_{11}C_{44} + C_{11}(C_{11} - C_{12} - 2C_{44})\cos 4\theta \right] (\varepsilon_{xx}^2 + \varepsilon_{yy}^2) \\ & - 2 \left[-C_{11}^2 - 3C_{11}C_{12} + 4C_{12}^2 + 2C_{11}C_{44} + C_{11}(C_{11} - C_{12} - 2C_{44})\cos 4\theta \right] \varepsilon_{xx}\varepsilon_{yy} \end{aligned} \right\}, \quad (4.6)$$

Hence, the driving force can be estimated analytically using linear elasticity as,

$$P = \frac{1}{4}(2C_{44} - C_{11} + C_{12})\sin^2(2\theta)(\varepsilon_{xx} - \varepsilon_{yy})^2, \quad (4.7)$$

where C_{11} , C_{12} and C_{44} are the elastic constants and $(2C_{44} - C_{11} + C_{12})$ is the measure of the elastic anisotropy of material. It is noted that the driving force is vanishing when $\varepsilon_{xx} = \varepsilon_{yy}$, and is maximized when $\theta = 45^\circ$. Based upon this calculation, we chose $\varepsilon_{xx} = -\varepsilon_{yy}$ in our simulation cell to maximize the driving force.

The accuracy of this calculation relies on the linearity of the stress-strain relation. Typical strains employed in our simulations are up to 2%, where the linearity of stress-strain relation is questionable. In order to take account the non-linear elasticity in the calculation of driving force, an alternative approach is applied. In this approach, a series of molecular dynamics simulations were performed in each grain to obtain the stress-strain curves; then, expand obtained stress in the power of strain, following equation:

$$\sigma(\varepsilon) = A\varepsilon + B\varepsilon^2 + \dots, \quad (4.8)$$

where A and B are constants. The stored elastic free energy in each grain was estimated using numerical integration under each stress-strain curve at a given strain level; and finally, the driving force was obtained by the difference of the stored elastic free energy between two grains, following equation:

$$P(\varepsilon) = \int_{-\varepsilon_0}^{\varepsilon_0} (\sigma_{xx}^{Grain2} + \sigma_{yy}^{Grain2} - \sigma_{xx}^{Grain1} - \sigma_{yy}^{Grain1}) d\varepsilon', \quad (4.9)$$

or

$$P(\varepsilon_0) = \frac{1}{2}(A_2 - A_1)\varepsilon_0^2 + \frac{1}{3}(B_2 - B_1)\varepsilon_0^3 + \dots, \quad (4.10)$$

where P is the elastic energy difference between the two grains (driving force) while Figure 4.2 indicates the deviation of stress-strain curve from linear region at large applied strain. The purple area indicates energy difference between the estimation from linear elasticity and the proposed simulation measurement.

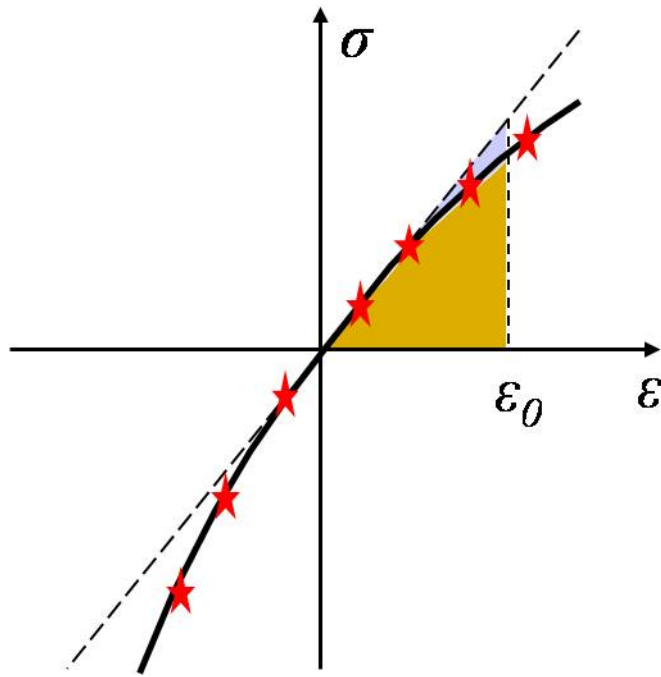


Figure 4.2 Illumination of deviation from linear elasticity. Brown area indicates the elastic energy obtained from measurement (non-linear elasticity) while the purple zone represents energy difference between linear elasticity estimation and measurement. Red stars are the measured stress when apply selected strain.

The obtained elastic energy difference between upper and lower grain (green zone) is illustrated in Figure 4.3 .

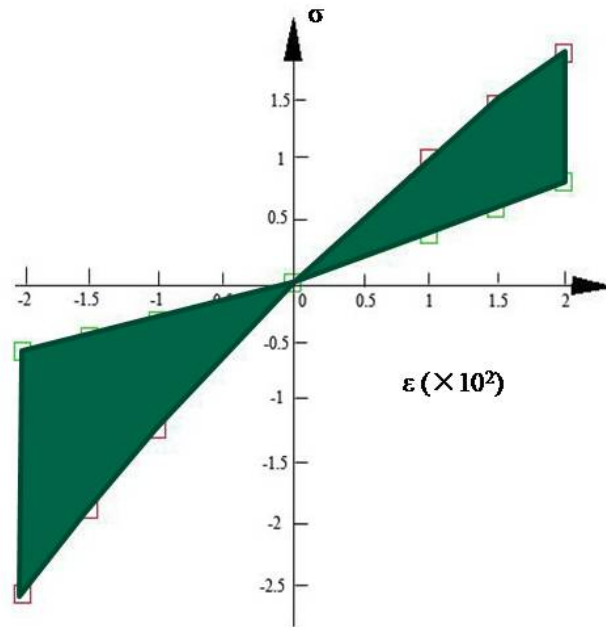


Figure 4.3 Obtained elastic energy difference (the green zone) between the two grains

Due to the deviation from linear elasticity, estimated driving force are, hence, different from measured one, shown in Figure 4.4. More details could be found in [17].

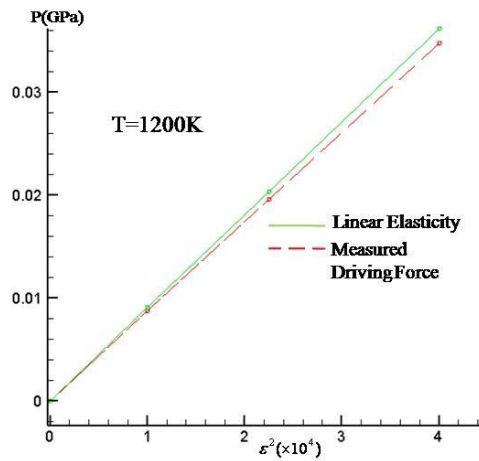


Figure 4.4 Illumination of driving force difference between linear elasticity estimation and measured driving force.

4.3 Grain Boundary Migration Velocity

Grain boundary velocity is obtained by linear fitting the plot of grain boundary position versus time, indicated by Figure 4.5. From the figure, we could observe that grain boundary reaches a steady-state migration while grain boundary migration rate is the slope of the linear fit of the grain boundary position versus time plot. By employing this method, velocity data at different temperature was applied strain were obtained for each selected twist boundary.

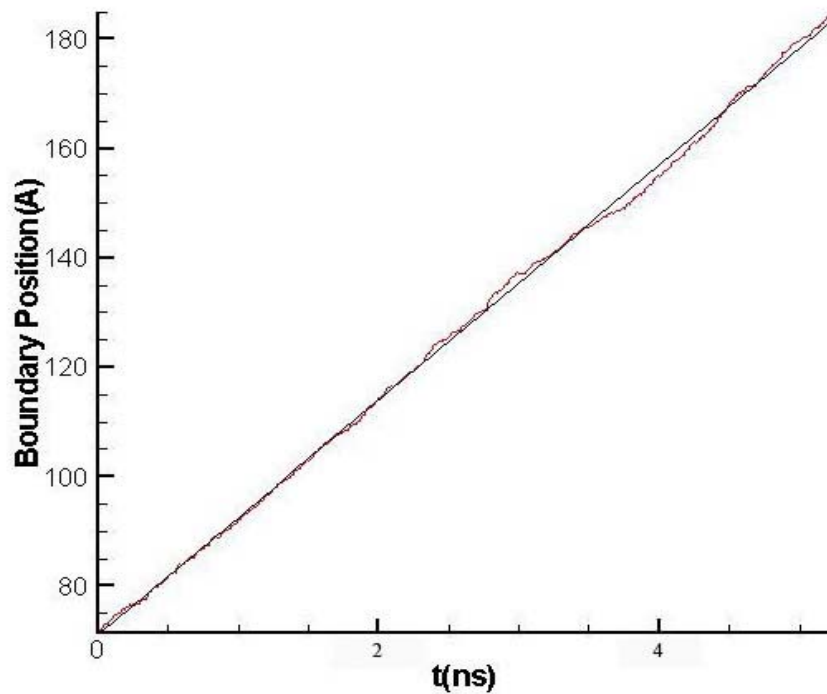


Figure 4.5 Linear fit of the grain boundary position versus time

4.4 Statistical Measures for Characterizing Atomic Motions during Migration

Previous simulation with respect to tilt grain boundary mechanism studies confirmed co-operative atomic motions within the grain boundary. Such motions

are named as collective string-motions [39-41, 64]. Figure 4.6 indicates the string motions found in tilt grain boundary where boundary region was blanked except tracked strings (colorful atoms linked with arrows). The upper and lower region of atoms, respectively, represent the atoms belonging to each grain in the bicrystal configuration [64]. Typically, string motions found in tilt grain boundaries are predominantly parallel to tilt axis.

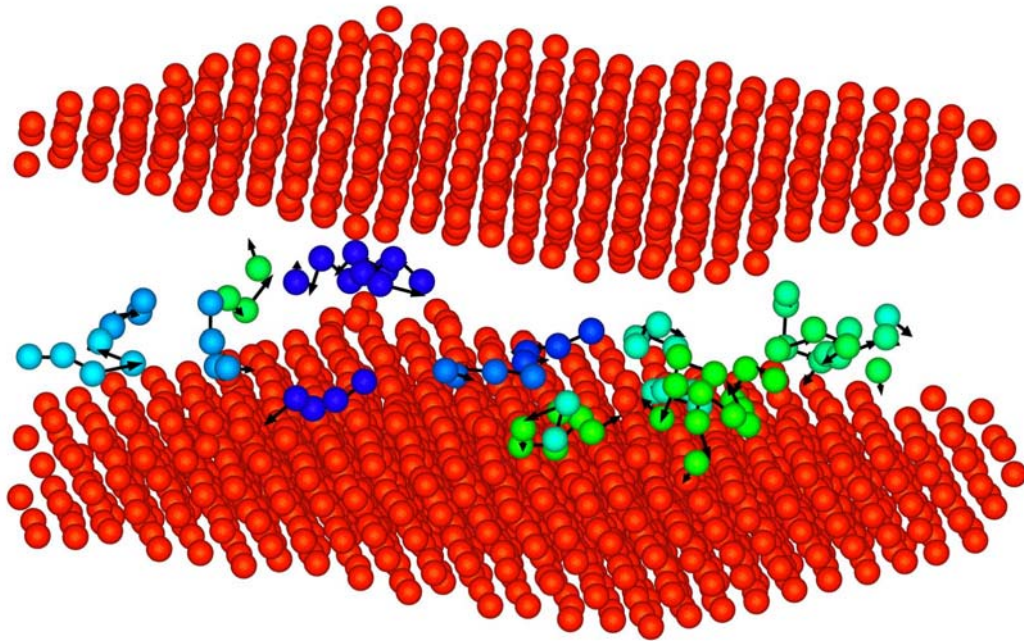


Figure 4.6 Collective string motions observed in a tilt grain boundary. Red atoms either belong to upper or lower grain while series of colorful (other than red) atoms indicate observed string motions. [64]

A quantitative measure [41] has been developed to characterize the string-like collective atomic motions within grain boundary plane. The criterion for

determining string-like atomic motions is as follows: first, mobile atoms should be identified. An atom will be treated as a mobile atom if its displacement in time interval Δt is larger than thermal vibration amplitude, but smaller than the second nearest neighbor distance, i.e., $0.35r_0 < |r_i(\Delta t) - r_i(0)| < 1.2r_0$. Next, mobile atom i and atom j can be identified as a pair or a string if they remain nearby as they move, i.e., $\min[|r_i(\Delta t) - r_j(0)|, |r_i(0) - r_j(\Delta t)|] < 0.43r_0$. The average string length then can be estimated as $\bar{n}(\Delta t) = \sum_{n=2}^{\infty} nP(n, \Delta t)$, where n is the number of atoms involved in a string and $P(n, \Delta t)$ is the probability of finding a string of length n in a time interval Δt .

Self-part van Hove correlation function $G_s(r, \Delta t)$ is employed to characterize the atomic displacement during grain boundary migration. $G_s(r, \Delta t)$ describes the probability distribution of an atom to be found from its original position by an amount of r after a time Δt . Mathematically, the van Hove correlation function can be written as:

$$G_s(\mathbf{r}, \Delta t) = \frac{1}{N} \left\langle \sum_{i=1}^N \delta(\mathbf{r}_i(\Delta t) - \mathbf{r}_i(0) - \mathbf{r}) \right\rangle, \quad (4.11)$$

When Δt is small, $G_s(r, \Delta t)$ is Gaussian, meaning harmonically localized motion. As time interval Δt increasing, generally, we will expect to observe non-Gaussian behavior. By looking at $G_s(r, \Delta t)$ at a different time interval, we can trace the path that the atom takes as it moves through the system and quantify these changes in terms of atomic displacement. It is noted that the atomic displacement is sensitive

to any rigid motion between two grains. To minimize the effect of grain boundary rigid motion during the atomic displacement calculation, we chose to fix the atomic positions of two layers of atoms near the top and bottom surfaces in the X - and Y -directions during simulations.

4.5 Simulation Results

4.5.1 Grain Boundary Mobility

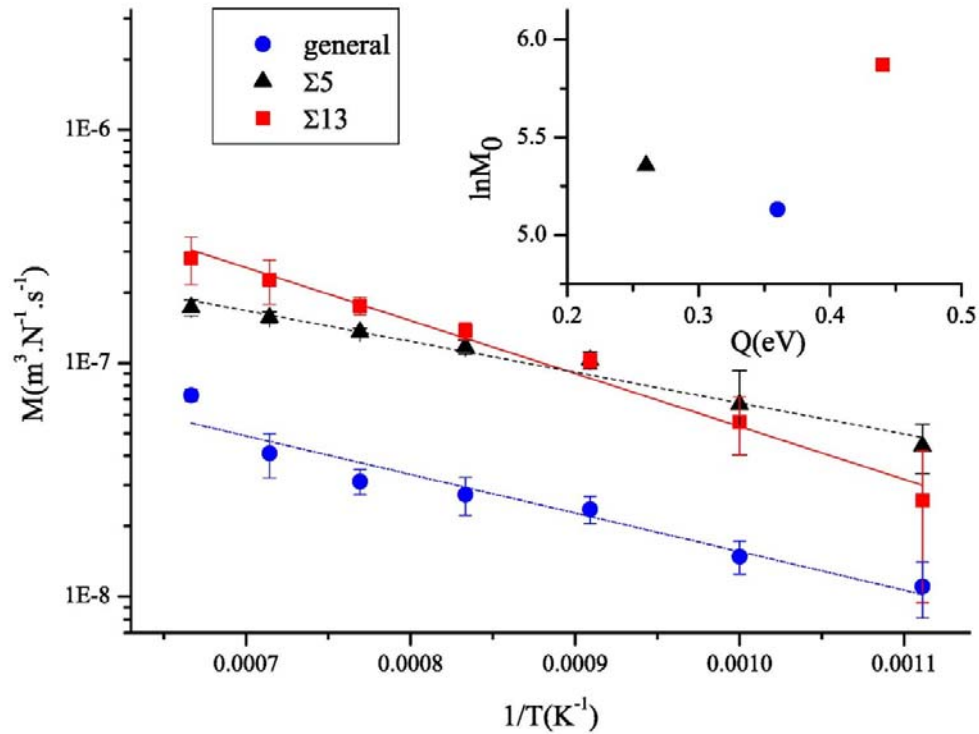


Figure 4.7 Logarithm of grain boundary mobility versus inverse temperature for $\Sigma 5$, $\Sigma 13$ and general twist boundaries. The inset shows logarithm of the pre-exponential factor as a function of the activation energy.

Figure 4.7 shows grain boundary mobility as a function of temperature for $\Sigma 5$,

$\Sigma 13$ and $\theta=40.23^\circ$ general high-angle twist grain boundaries. In order to get mobility data at each temperature, shown in Figure 4.7, we first need to calculate driving force under different strains. As a typical example, driving force data for $\Sigma 5$ [001] twist boundary at 1300K is illustrated in Table 4.1

Temperature	Strain	Grain2 (Upper)		Grain1 (Lower)		Driving Force (GPa)
		σ_{xx} (GPa)	σ_{yy} (GPa)	σ_{xx} (GPa)	σ_{yy} (GPa)	
1300K	0.01	1.2136	-1.3870	0.4951	-0.4061	0.008439
	0.015	1.7366	-2.1687	0.7510	-0.5809	0.019065
	0.02	2.2166	-2.9996	1.0263	-0.7216	0.034032

Table 4.1 Data for calculating driving force at 1300K for $\Sigma 5$ [001] twist boundary

Thus, according to obtained driving force and measured grain boundary velocities, we could calculate the mobility. Mobility data for 1300K $\Sigma 5$ [001] twist boundary is also provided in Table 4.2

T	Strain	Time (ns)	Velocity(m/s)	DF (GPa)	Mobility
1300K	0.02	10	4.6308	0.034032	136.07
1300K	0.015	11	2.5321	0.019065	132.81
1300K	0.01	11	1.1723	0.008439	138.91

Table 4.2 Obtained mobility data at 1300K for $\Sigma 5$ [001] twist boundary

Hence, the mobility at each temperature is obtained by averaging over simulation of migration at three different driving forces (i.e., $\varepsilon=1\%$, $\varepsilon=1.5\%$ and $\varepsilon=2\%$). Each simulation is performed for at least 10 ns to ensure that grain boundary migrates up to 14 nm. The error estimate is based upon a 95%

confidence interval. For each misorientation, the mobility $\ln M$ shows reasonable linearity with the inverse temperature $1/T$. This implies that grain boundary mobility can be described as an Arrhenius function of temperature, as suggested in Eq. (4.1). Linear fitting of the data set to the form $M = M_0 e^{-Q/k_B T}$ allows us to extract the activation energy for grain boundary migration Q (from the slope) and the pre-exponential factor M_0 (from the intercept). The activation energies for $\Sigma 5$, $\Sigma 13$ and general high-angle grain boundaries are $0.26 \pm 0.019 \text{ eV}$, $0.45 \pm 0.026 \text{ eV}$ and $0.36 \pm 0.022 \text{ eV}$, respectively. These values are in good agreement with our previous simulations of grain boundary migration in $\Sigma 5$ tilt boundaries [65], where the activation energies for migration fall into a range from 0.2 eV to 0.4 eV . Since all the activation energies are non-zero, we can conclude that grain boundary migration for these twist boundaries is thermally activated process. It is also noted that the Arrhenius plot of $\ln M$ vs. $1/T$ for $\Sigma 5$ and $\Sigma 13$ boundaries crosses at 1100 K (general boundary and $\Sigma 5$ could have an intersection above the melting point and general boundary and $\Sigma 13$ could intersect at a much lower temperature). This is the so-called compensation temperature, as discussed in previous chapter [66], a typical experimentally observed correlation [30]. The inset of Figure 4.7 plots logarithm of the pre-exponential factor M_0 versus activation energy Q for three twist boundaries. It is clear that the data sets cannot be described as a linear relationship. This implies the atomistic mechanisms by which grain boundary migrates might be different between these boundaries.

Moreover, while the activation energies for three misorientations are relatively close, the general grain boundary shows substantially lower mobility at all temperatures interested. This suggests that the migration mechanism for non- Σ (general high angle) twist boundaries might be different from Σ twist boundaries ($\Sigma 5$ and $\Sigma 13$).

4.5.2 Grain Boundary Kinetics

Next, we will employ the methods introduced in Section 4.4 to identify the atomistic mechanisms for grain boundary migration in twist boundaries. The temperature $T=900\text{K}$ was chosen in the investigation to ensure that grain boundaries migrate by enough amount of distance with MD time scales but that the natural random walk of the boundary due to thermal fluctuation is small. The applied strain for $\Sigma 5$, $\Sigma 13$ and general twist boundaries are 1.5%, 2.0% and 1.5%, respectively.

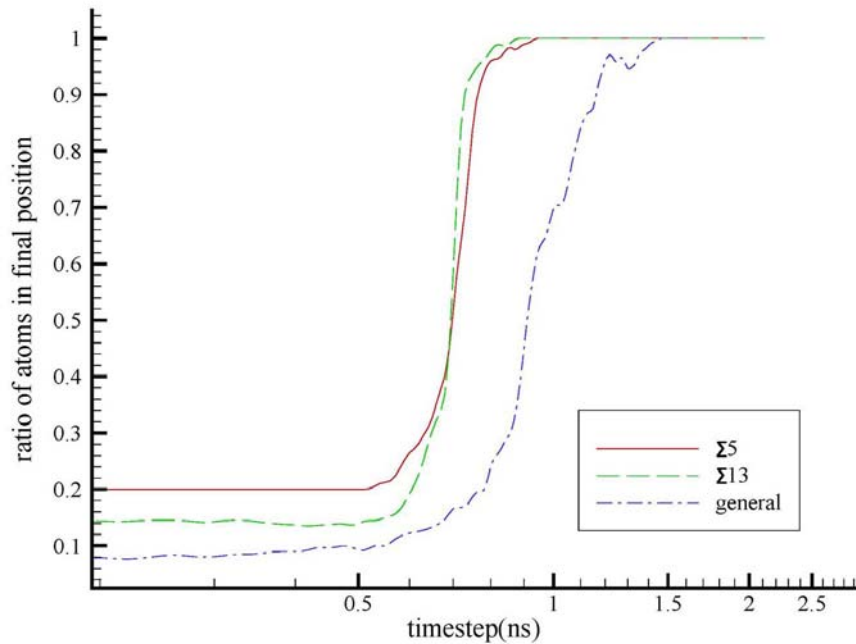


Figure 4.8 Kinetics of the three selected twist boundary at 900K.

The choice of different strain in different boundaries is to ensure the driving force is similar between different boundaries. Figure 4.8 indicates migration kinetics obtained from the three selected twist boundaries. For each type of boundary, several layers' kinetics were obtained and averaged to acquire averaged kinetics shown in Figure 4.8. A few layers on the path of migration for each selected grain boundary were chosen. The selected layers, which belong to upper grain with original misorientation θ , would finally become layers with unrotated configuration. The ratio of atoms changing from rotated configuration to the final configuration was plotted versus time for each type of selected twist boundary. For each observed plane, its configuration was averaged over several consecutive

timesteps. On the other hand, the reference was selected as the layer close to observed plane with observed plane's final configuration, whose configuration was also obtained via averaging. When some atoms in the observed planes approximately match the atoms in reference planes, these atoms in observed plane would be labeled as atoms with final orientation (unrotated). From the figure, we could see that, in the beginning, $\Sigma 5$ and $\Sigma 13$ both have a certain amount of atoms with final misorientation, which, respectively, matches the percentage of CSL atoms in each grain boundary plane. As for general boundary, the initial ratio is due to the error brings by thermal vibration. Theoretically, there should be no atoms with final misorientation for general twist boundary plane. These observations suggest CSL atoms are simply involved in thermal vibration around their original positions since the ratio of atoms with final orientation for $\Sigma 5$ and $\Sigma 13$ twist boundaries always maintain the same before migration started. In addition, this figure confirms that general twist boundary has a relatively lower mobility.

4.5.3 Single Atomic Motions

Figures 4.9, 4.10 and 4.11, respectively, show the self-part of van Hove correlation function (displacement distribution function) at eight different time intervals Δt for $\Sigma 5$, $\Sigma 13$ and general high-angle twist grain boundaries at 900K. In all cases, at small time interval the displacement distribution function is Gaussian since the atomic motions are simply harmonic oscillation around their equilibrium

positions. Hence the peaks at $r \sim 0.5\text{\AA}$ in three cases correspond to the atomic vibration amplitude at $T = 900\text{K}$. As the time interval increases, the displacement distribution function starts to develop new peaks at $r=r_0$ and $r=a$, where the r_0 corresponds to the first nearest neighbor distance of the fcc nickel and the a corresponds to the lattice parameter (the second nearest neighbor distance). In previous simulations [39] of tilt grain boundary it has been demonstrated that the displacements at r_0 and a are most likely the atomic motion associated with grain boundary self-diffusion. While the displacement distribution functions exhibit some similarities, significant differences are shown as time interval becomes larger among three boundaries.

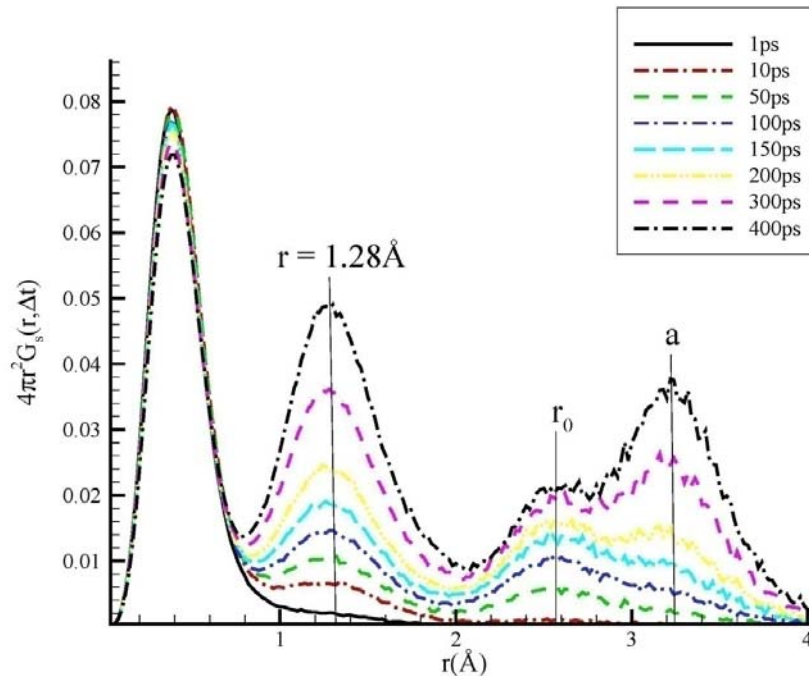


Figure 4.9 The displacement distribution function G_s at eight different time intervals Δt for

$\Sigma 5$ boundary

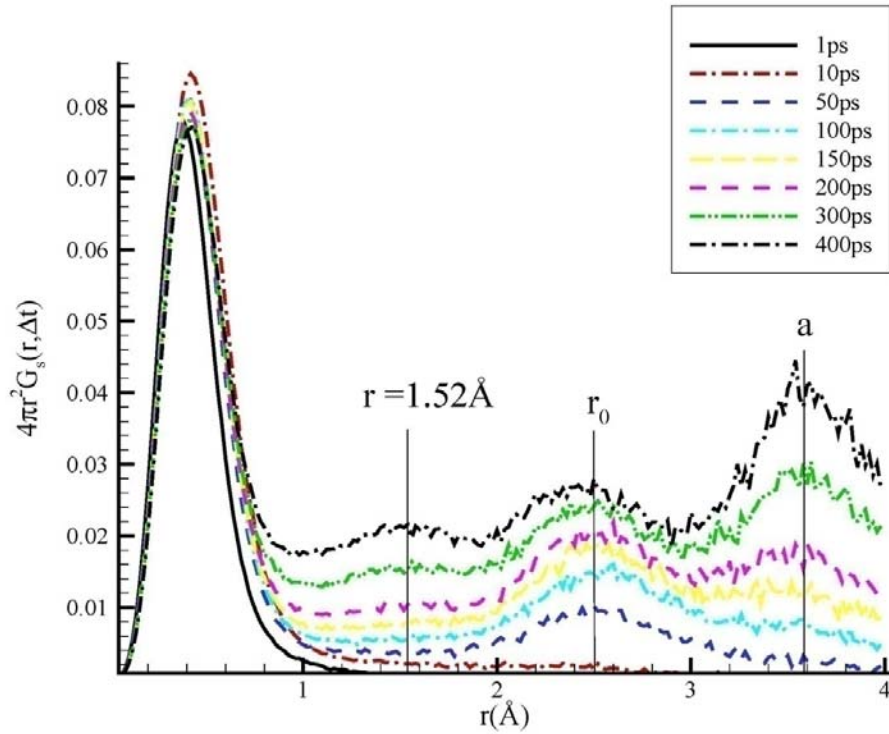


Figure 4.10 The displacement distribution function G_s at eight different time intervals Δt for $\Sigma 13$ boundary

Figure 4.9 shows the displacement distribution function of the $\Sigma 5$ twist grain boundary. A strong new peak centering at $r=1.28\text{\AA}$ appears when $\Delta t > 50\text{ps}$. The new peak suggests that substantial amount of atoms displace such a distance after a certain time, where this displacement (short jump) is only half length of the first nearest neighbor distance r_0 . Similar to the $\Sigma 5$ twist boundary, a new but broader peak centering at $r=1.52\text{\AA}$ develops in the $\Sigma 13$ twist grain boundary, as shown in Figure 4.10. Both peaks found in $\Sigma 5$ and $\Sigma 13$ twist boundaries are similar to our previous observations in tilt boundaries [41], where the “short jump” corresponds to single atom hop across the grain boundary. Figure 4.11 shows the displacement

distribution function in the general high-angle twist grain boundary. It is surprising that other than the peaks at $r \sim 0.5 \text{ \AA}$, $r = r_0$ and $r = a$, no “short jump” is discovered. This indicated that no specific atomic displacements less than first nearest neighbor take place in general high-angle twist boundary. The differences found in displacement distribution function between Σ boundaries and non- Σ boundaries suggest that the atomic motion that governs grain boundary migration is different and it is sensitive to grain boundary symmetry. Next, we would examine where the “shot jump” in Σ grain boundaries originates.

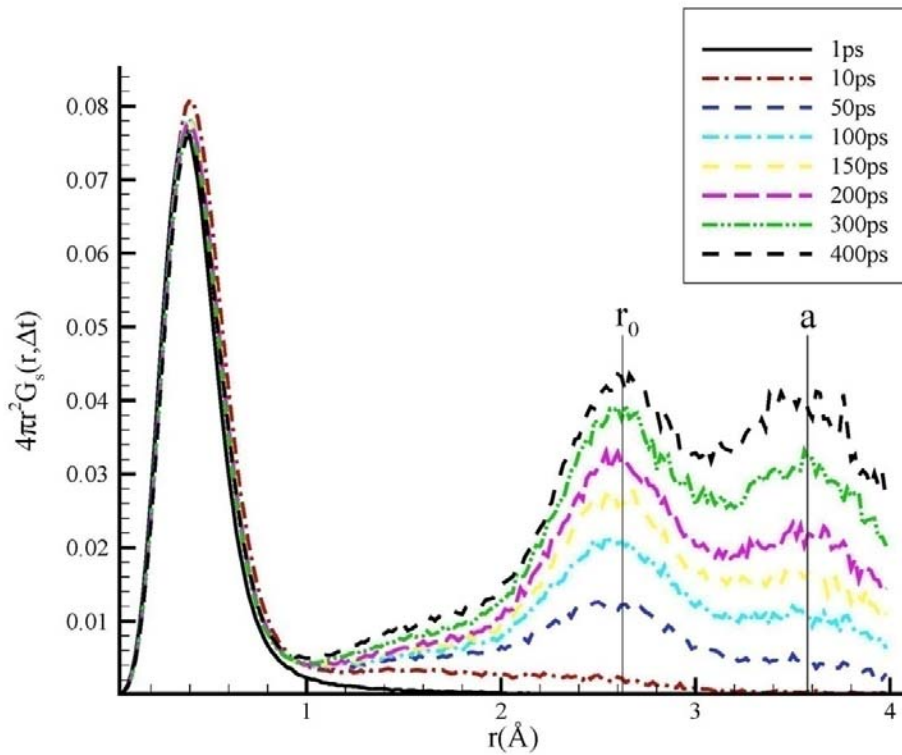


Figure 4.11 The displacement distribution function G_s at eight different time intervals Δt for general high angle twist boundary.

Temporal evolution of atomic configurations and angular distribution

function are employed to determine the origin of the “short jump” found in the displacement distribution function. The temporal evolution of atomic configurations with a X - Y plane view of a single (002) atomic plane contains thousands of individual atomic configurations separated in time interval by 0.2 ps over 2 ns period of time. The atomic positions are colored by the time, i.e., light – early time and dark – later time. Since such a figure shows the motion of all atoms over a long period of time, it provides information on the atomic trajectory in a statistical sense. Angular distribution function is used to examine whether certain “short jump” within grain boundary plane (the X - Y plane) has angular correlation and whether such correlations are related to grain boundary structures. In order to calculate the angular distribution function, we first identify the “displaced” atoms if the displacement is within a selected range (e.g., for $\Sigma 5$ grain boundary, we choose $0.78\text{\AA} < r < 1.78\text{\AA}$), then the displacement vectors are projected onto the X - Y plane and an angle α_i for the “displaced” atom i is measured with respect to the X -direction. Finally, the angular distribution function $\gamma(\alpha)$ is calculated as,

$$\gamma(\alpha, \Delta t) = \frac{1}{N} \left\langle \sum_{i=1}^N \delta(\alpha - \alpha_i) \right\rangle. \quad (4.10)$$

The time interval Δt is chosen to be 400ps in the present work.

Figure 4.12 shows the temporal evolution of atomic configurations in the X - Y plane for the $\Sigma 5$ twist boundary. Only an enlargement of a small part of the entire grain boundary is shown. It is clear that the dark cluster of atoms and light cluster

of atoms represent the orientation of the lower and the upper grains, respectively. The black triangles represent the initial atomic positions of the upper grain while the white circles indicate the final atomic positions of the lower grain. Coincidence site lattice, the positions that light cluster of atoms are overlapped with the dark cluster of atoms, is connected by the dashed line.

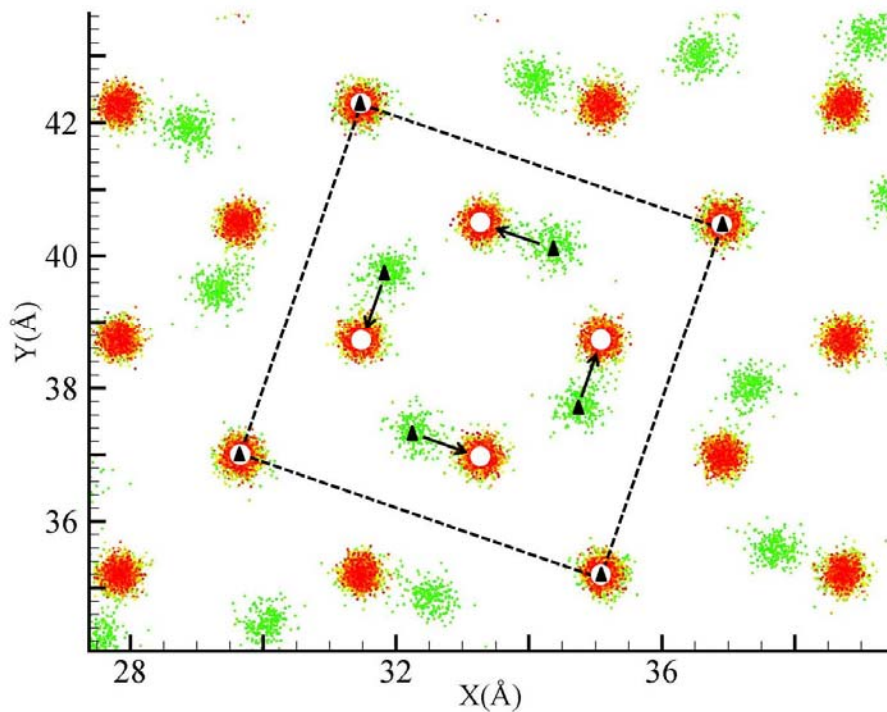


Figure 4.12 Boundary plane view (X - Y) of superimposed atomic positions every 0.2 ps for 1000 time intervals for $\Sigma 5$ twist boundary. The atoms are colored according to time, where darkest (red online) and lightest (green online) represent starting and finishing times, respectively. The dashed square indicates the unit cell of the coincidence site lattice and arrows denote the single atomic hopping path.

Since in this figure we know where each atom begins its trajectory and ends

its trajectory, we can determine a statistically meaningful atomic jump path. The black arrows indicate such a jump path. There is no displacement or jump involved in those atoms in the CSL site. This jump path is consistent with the so-called DSC lattice [2], where the length of the vector is estimated to be 1.14 Å [2]. This is a good agreement with the peak at $r=1.28\text{Å}$ in the displacement distribution function, shown in Figure 4.9. Figure 4.13 shows the angular distribution function for the atoms with displacements in a range of 0.78Å and 1.78Å. The peaks at $\theta=20^\circ$, $\theta=110^\circ$, $\theta=200^\circ$ and $\theta=290^\circ$ in the angular distribution function suggest that these four angles or directions are taken by the most atoms with a displacement in a range of 0.78Å and 1.78Å [second peak in Figure 4.9]. In addition, these four directions are also reasonable matching with the jump paths suggested in Figure 4.12.

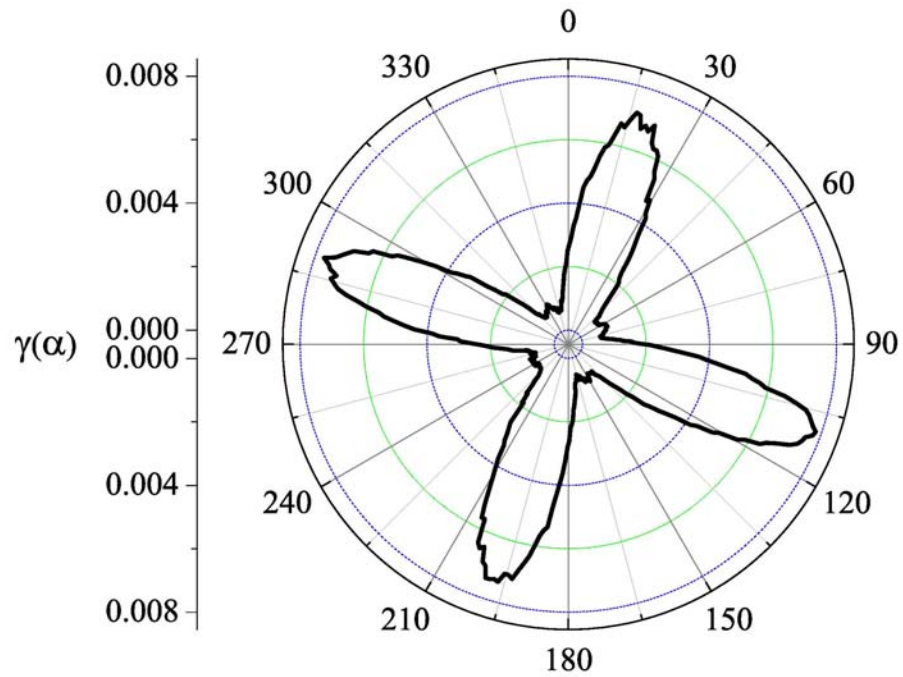


Figure 4.13 Angular distribution function of the atoms with displacement around the peak centered at $r = 1.28\text{\AA}$ in Figure 4.9 (figure of $\Sigma 5$ twist boundary van Hove correlation function).

Therefore, both the temporal evolution of atomic configuration and the angular distribution function confirm the “short jump” path within a CSL cell for $\Sigma 5$ twist boundary. Since such short jumps eventually lead to grain boundary migration, we believe they are the controlling atomic motions that govern grain boundary migration in $\Sigma 5$ twist boundary.

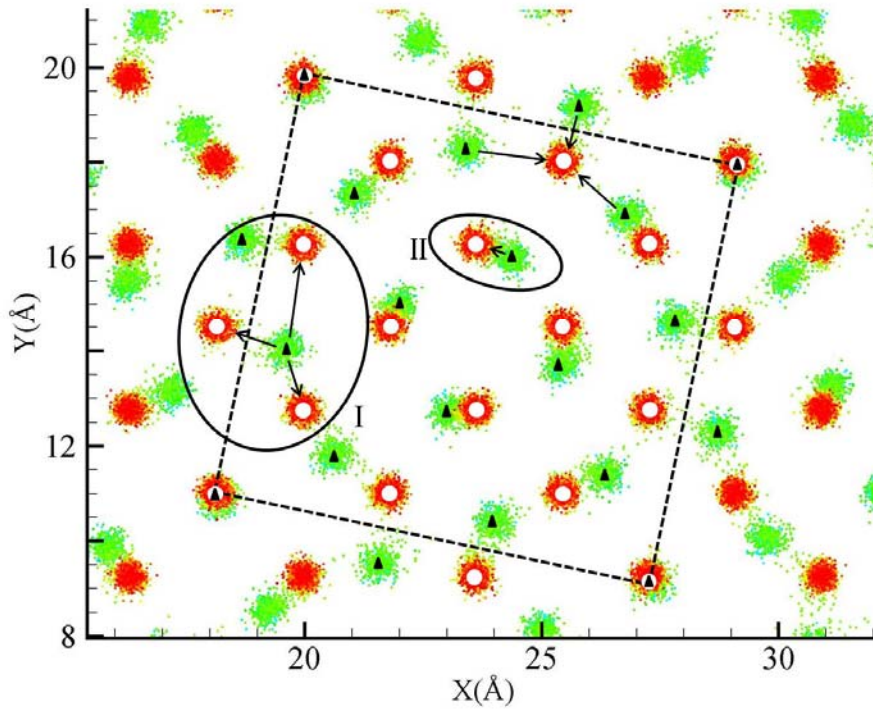


Figure 4.14 Boundary plane view (X - Y) of superimposed atomic positions every 0.2 ps for 1000 time intervals for Σ_{13} twist boundary. The dashed square indicates the unit cell of the coincidence site lattice and arrows denote the possible single atomic hopping directions.

Figure 4.14 shows the temporal evolution of atomic configurations in the X - Y plane for the Σ_{13} twist boundary. Similar to the Σ_5 twist boundary, the CSL site can be defined and indicated by the dashed line. Nevertheless, short jump paths are difficult to determine. The angular distribution function of atoms having displacement between 1.02\AA and 2.02\AA is shown in Figure 4.15. Compared with the angular distribution function for the Σ_5 boundary, more angles or directions for the short jump in the Σ_{13} boundary are observed. Based on the information in

Figure 4.14 and 4.15, we can determine the possible jump path for the $\Sigma 13$ boundary, indicated by the black arrows. The distance of the possible displacements ranges from 0.72\AA to 2.05\AA . This is the reason why we observe a much broader second peak in the $\Sigma 13$ twist boundary in the displacement distribution function [Fig. 4.10]. The possible short jump displacement can be divided into two types: i) Type I is the outer ring jump with relatively large displacement (i.e., $>1.02\text{\AA}$), and ii) Type II is the inner ring jump with relatively small displacement (i.e., $\sim 0.72\text{\AA}$).

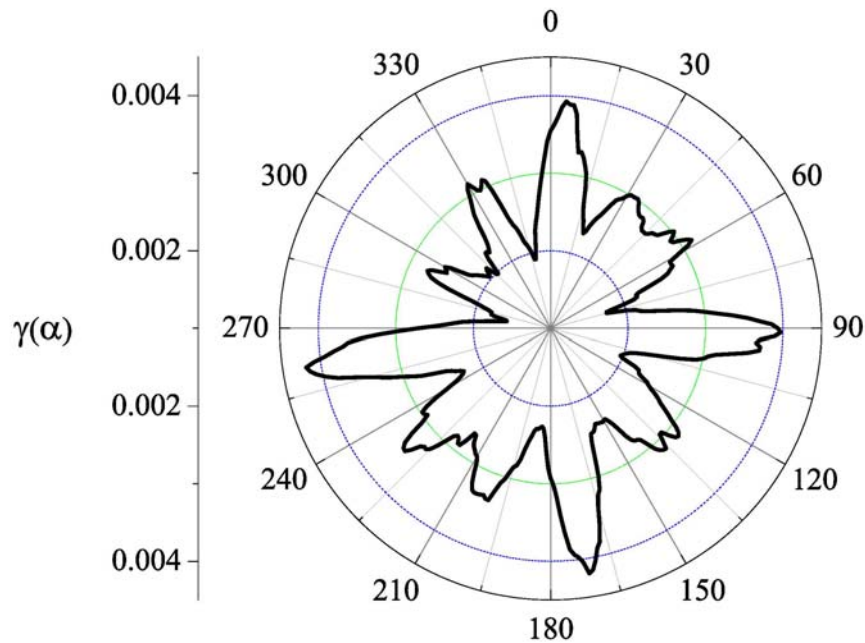


Figure 4.15 Angular distribution function of the atoms with displacement around the peak centered at $r=1.52\text{\AA}$ in Figure 4.10 (figure of $\Sigma 13$ twist boundary van Hove correlation function).

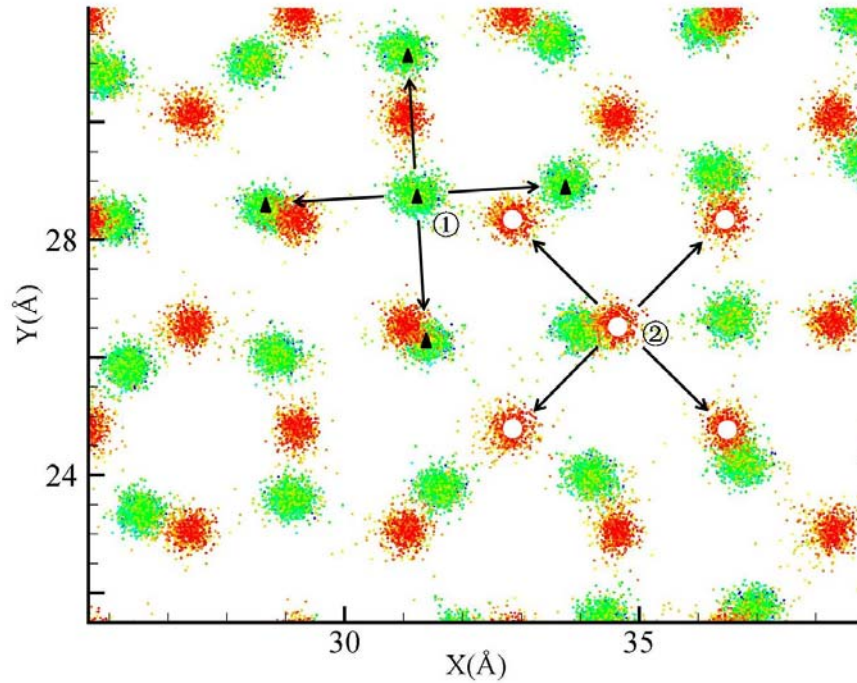


Figure 4.16 Boundary plane view (X - Y) of superimposed atomic positions every 0.2 ps for 1000 time intervals for general high angle twist boundary. The arrows denote the possible single atomic hopping directions.

Figure 4.16 shows the temporal evolution of atomic configurations in the X - Y plane for the general high angle twist boundary. Although this figure also suggests possible short jump paths from the atomic trajectory, the van Hove correlation function indicates no significant displacements that are less than atomic distance take place during migration. Therefore, short jump is not important for the general high angle twist boundary. Figure 4.17 shows the angular distribution function of the atoms having displacement of the first nearest neighbor distance. Surprisingly, these first nearest neighbor jumps within general grain boundary are not random,

rather, the directions coincide with the crystallographic orientation of the upper or lower grain. This suggests that the atom within grain boundary is likely to jump into its nearest neighbor in its own sublattice, as illustrated by atom (1) and atom (2) in 4.16.

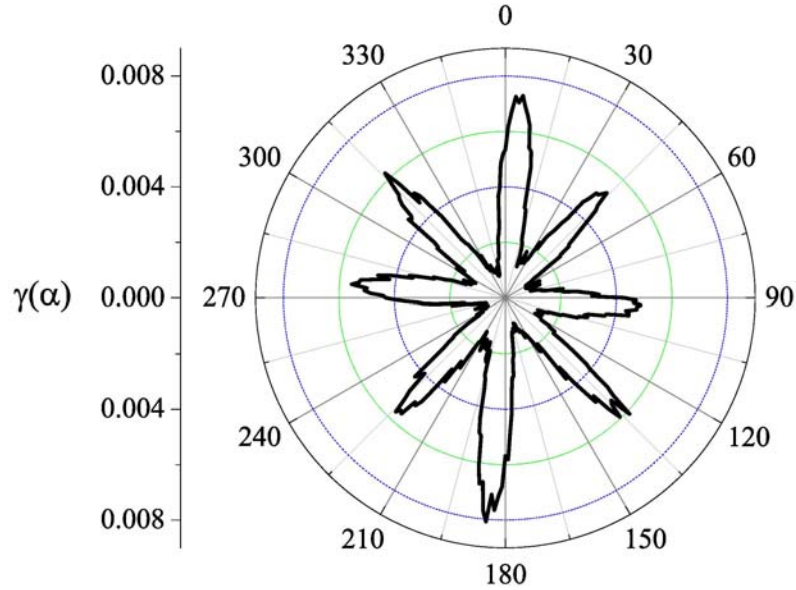


Figure 4.17 Angular distribution function of the atoms with displacement around the peak centered $r=r_0$ in Figure 4.11 (figure of general twist boundary van Hove correlation function).

4.5.4 String-like Cooperative Motions

String-like cooperative motion is an intrinsic feature of grain boundary motion that may greatly influence the dynamics of grain boundary during migration [41, 64]. For the typical string-like cooperative motions within grain boundary, string length will increase with increasing time interval Δt until it reaches a maximum at $\Delta t = t^*$, and then it starts to decay. The choice of t^* for

general twist [001] grain boundary is indicated by Figure 4.18.

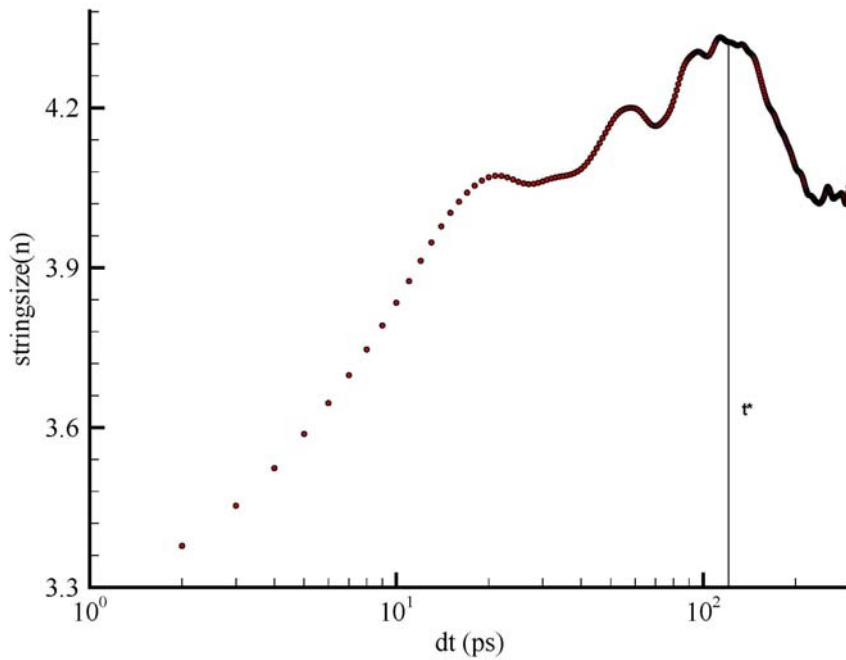


Figure 4.18 Selection of t^* when string size reaches maximum

At small and large Δt , the atomic displacements exhibit inertial and Brownian (both are uncorrelated), respectively, while between the two extremes the atomic displacements develop correlation and such a correlation reaches a maximum at $\Delta t = t^*$. Figure 4.19, 4.21 and 4.23 show the position of atoms in strings of length larger than three at $\Delta t = t^*$ in the X - Y plane for $\Sigma 5$, $\Sigma 13$ and general twist boundaries at $T=900\text{K}$ when the average grain boundary position has moved approximately 10 \AA along the Z -direction.

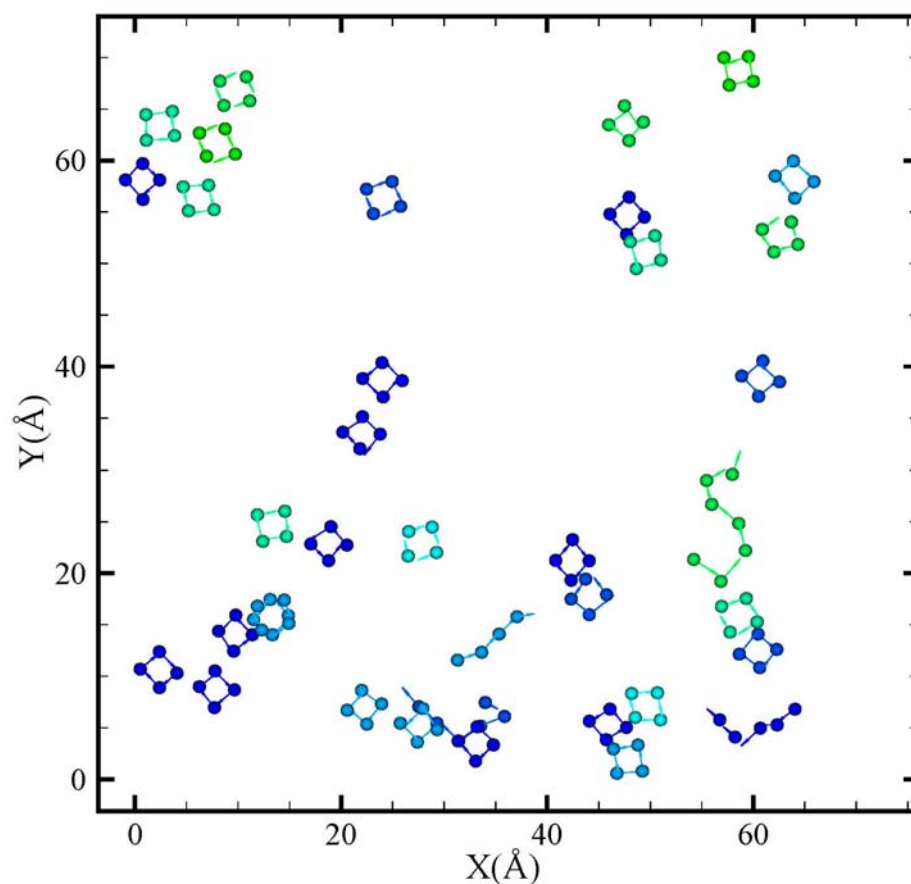


Figure 4.19 Identification of all of the atoms that are members of strings of length greater than three at $\Delta t = t^*$ in $\Sigma 5$ boundary X - Y plane when the grain boundary migrates approximately 10\AA . Different colors represent individual strings and the arrows point to the positions where atoms end.

In Figure 4.19, the string-like cooperative motions in the $\Sigma 5$ twist grain boundary at $\Delta t = 113$ ps are shown, where 4-atom strings are found to be dominant. Two types of 4-atom string can be identified based on their orientation. Each of the string orientation coincides with the crystallographic orientation of the upper or lower grain. However, these 4-atom strings are not related to the 4-atom

shuffles mechanisms suggested by the previous works [14, 42, 43] simply because they do not involve any local crystal orientation change. Indeed, the definition of 4-atom shuffles is slightly different from the definition of the strings in this work. In a 4-atom string, each atom tends to jump into the position occupied by its member and the displacement is around the atomic distance, while in 4-atom shuffles, each atom tends not to jump into the position occupied by its member and the displacement is only half of the atomic distance. Our observation of the strong second peak ($r \sim 1.28 \text{ \AA}$) in the displacement distribution function and “short jump” path in X - Y plane are actually in accordance with the definition of 4-atom shuffles. One obvious question is “Are these ‘short jump’ part of 4-atom shuffles?” In order to answer this question, we performed additional string analysis based on the definition of 4-atom shuffles. In this analysis, atoms were treated as mobile if a “short jump” took place, i.e., $0.78 \text{ \AA} < |r_i(\Delta t) - r_i(0)| < 1.78 \text{ \AA}$ and then mobile atom i and j can be identified as collective if the distance between them at Δt was within a certain value. Figure 4.19 shows the position of atoms in 4-atom shuffles at $\Delta t = 3 \text{ ps}$ in the X - Y plane [a (002) atomic plane] for $\Sigma 5$ grain boundary over a period of 200ps. Atoms are colored by the time. This figure confirms that 4-atom shuffling motions are dominant mechanism for grain boundary migration in $\Sigma 5$ twist boundary as suggested by other researchers [14, 42, 43].

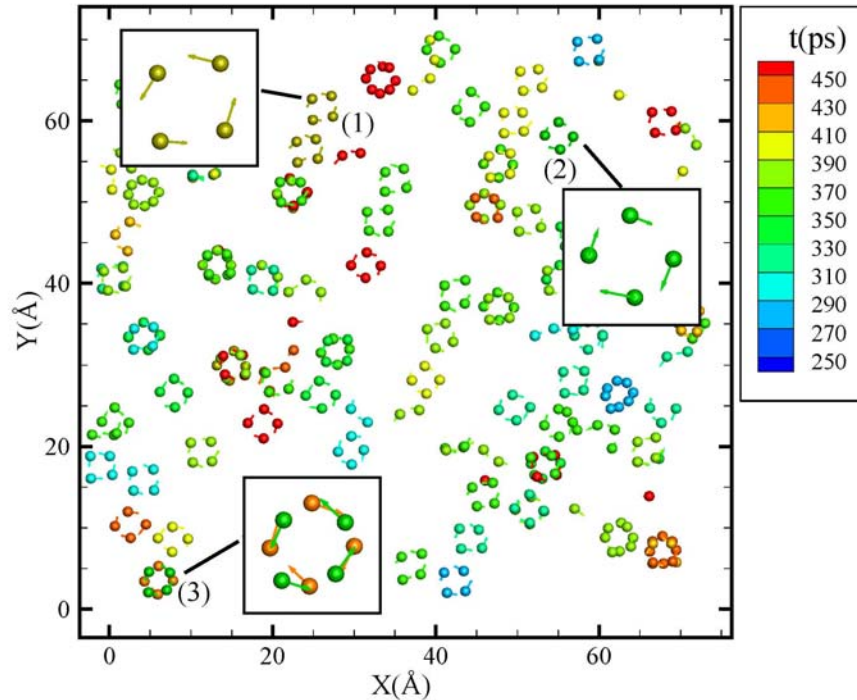


Figure 4.20 collective “short jump” in $\Sigma 5$ boundary X - Y plane at $\Delta t=3\text{ps}$. Atoms are colored by time and the arrows point to the positions where atoms end.

Examination of Figure 4.20 confirms three different types of 4-atom shuffles, i.e., (1) shuffles associated with orientation change from the upper crystal to the lower crystal, (2) shuffles associated with orientation change from the lower crystal to the upper crystal, and (3) reversible shuffles associated with orientation change from back and forth. It is also noted that compared with the correlation time ($\Delta t= 113\text{ps}$) for 4-atom string motion, the correlation time ($\Delta t= 3\text{ps}$) for the 4-atom shuffles is extremely short. Hence, the nature of the reversible shuffles and the short correlation time suggest the 4-atom shuffle motions are one type of intrinsic atomic motions in $\Sigma 5$ twist boundary. In addition, the color (time)

distribution provides us the information of whether or not the individual 4-atom shuffles are correlated.

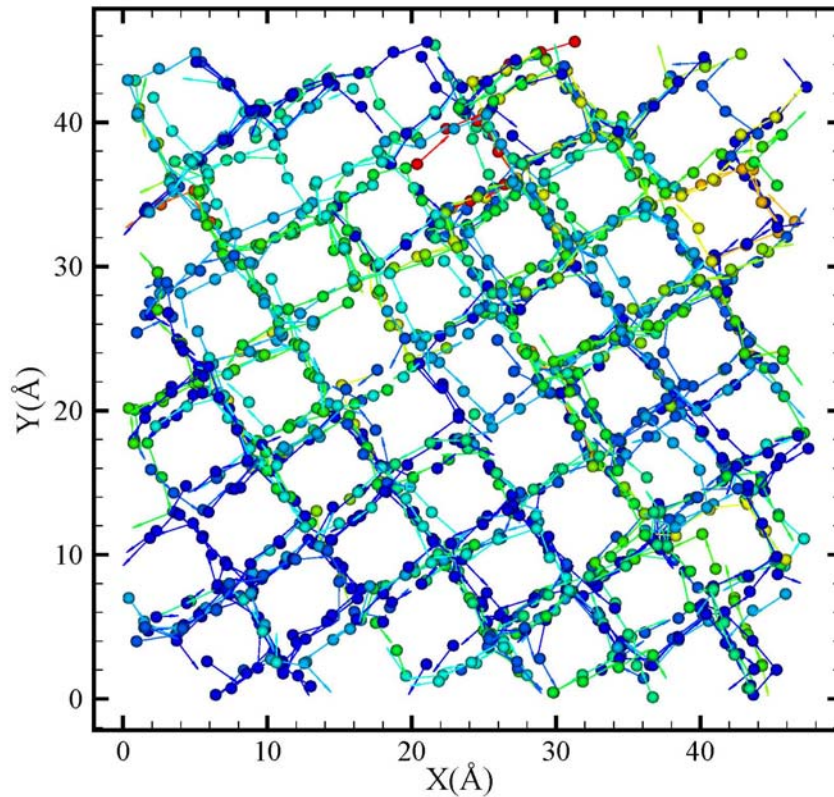


Figure 4.21 Identification of all of the atoms that are members of strings of length greater than three at $\Delta t = t^*$ in $\Sigma 13$ boundary X - Y plane when the grain boundary migrates approximately 10\AA . Different colors represent individual strings and the arrows point to the positions where atoms end.

Examination of Figure 4.20 shows that the color of 4-atom shuffles is well mixed, or uncorrelated. Therefore, since there is no clear correlation between individual 4-atom shuffles, the simulation result seems not support the idea that grain boundary migration in $\Sigma 5$ twist boundary occur by the propagation of kinks

along ledges, as suggested by [14, 42, 43].

Figure 4.21 demonstrates the string-like cooperative motions in the $\Sigma 13$ twist grain boundary at $\Delta t = 63$ ps. Compared with the cooperative string motions in the $\Sigma 5$ twist boundary, such motions in the $\Sigma 13$ boundary are much stronger and the overall string-like motion seems to form a network-like structure. The structure of low angle twist grain boundary ($\theta < 15^\circ$) can be described in terms of an array of screw dislocations [9] and intuitively, such dislocation lines can provide easy paths for the atomic displacement within grain boundary. The spacing d between screw dislocations in this description [67] can be expressed as:

$$d = \frac{\mathbf{b}}{2 \sin(\theta / 2)} \quad (4.11)$$

where \mathbf{b} is the Burgers vector ($\mathbf{b} = \frac{a}{2}[110]$ here) and θ is the misorientation angle.

It is noted that d decays as θ increases, and eventually the screw dislocation cores will overlap when θ is large enough. Therefore, it is difficult to identify the screw dislocation network for twist grain boundary when $\theta > 15^\circ$, while different techniques [14] were successful in determining such structures when $\theta < 15^\circ$ in previous simulations. As shown in Figure 4.21, the string-like cooperative motions tend to form regular channels in the $\Sigma 13$ twist grain boundary ($\theta = 22.63^\circ$). The average spacing between the nearby channels is 6.46 \AA , which is in excellent agreement with $d = 6.45 \text{ \AA}$, as suggested by Eq. (4.11). This agreement confirms that the network shown in Figure 4.21 represents the screw dislocation network of

$\Sigma 13$ twist grain boundary. This also implies that string-like cooperative motions are likely to take place along the dislocations cores. Although grain boundary dislocation structure is hard to obtain in the $\Sigma 13$ twist grain boundary using conventional structural measures [14], grain boundary dynamic motions (string-like cooperative motion) are proven to be an effective alternative way to determine such structures. Since the “short jump” in the $\Sigma 5$ twist boundary is intrinsic multiple atoms shuffling motion, it is of interest to know whether such shuffling motions are also dominant in the $\Sigma 13$ boundary and whether the “short jump” found in $\Sigma 13$ boundary is correlated.

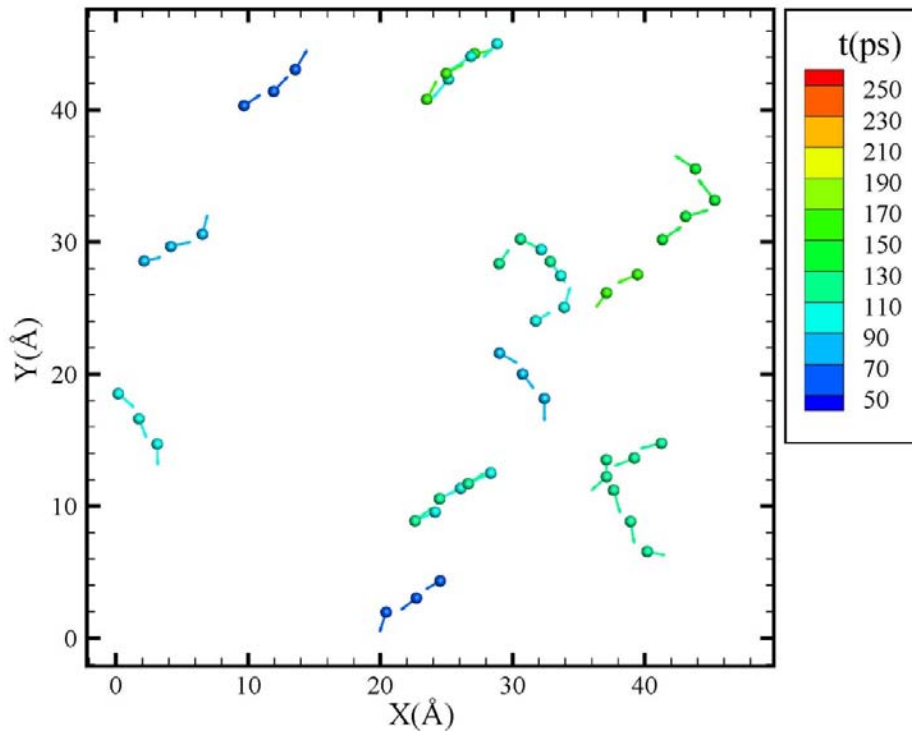


Figure 4.22 collective “short jumps” in $\Sigma 13$ boundary X - Y plane at $\Delta t=10$ ps. Atoms are colored by time and the arrows point to the positions where atoms end.

Figure 4.22 demonstrates the position of atoms in atomic “shuffles” at $\Delta t = 10\text{ps}$ in the X - Y plane [a (001) atomic plane] for $\Sigma 13$ grain boundary over a period of 200ps. As suggested by [14], it is not surprising that no 4-atom atomic shuffling motions were observed. Meanwhile, those captured atomic “shuffles” also tend to align in the screw dislocation cores. Therefore, it is evident that the “short jump” identified in the $\Sigma 13$ twist boundary is mostly single atom jump.

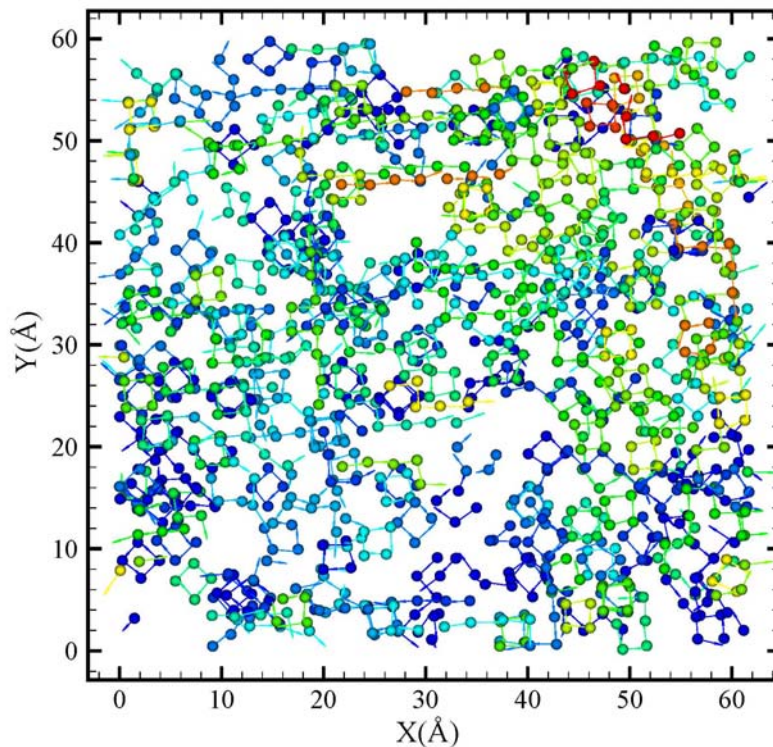


Figure 4.23 Identification of all of the atoms that are members of strings of length greater than three at $\Delta t = t^*$ in general boundary X - Y plane when the grain boundary migrates approximately 10\AA . Different colors represent individual strings and the arrows point to the positions where atoms end

Similar string motions in the general high-angle twist boundary are shown in

Figure 4.23. Compared with the $\Sigma 5$ and the $\Sigma 13$ twist boundaries, the non- Σ general boundary exhibits significantly stronger string-like cooperative motions during migration. However, the strings in the general twist boundary appear more randomly distributed and no regular network or patterns are observed. No additional 4-atom shuffle analysis is needed in the general twist boundary since the lack of “short jump”.

4.5.5 String Motion and Shuffling Motion in Stationary Boundaries

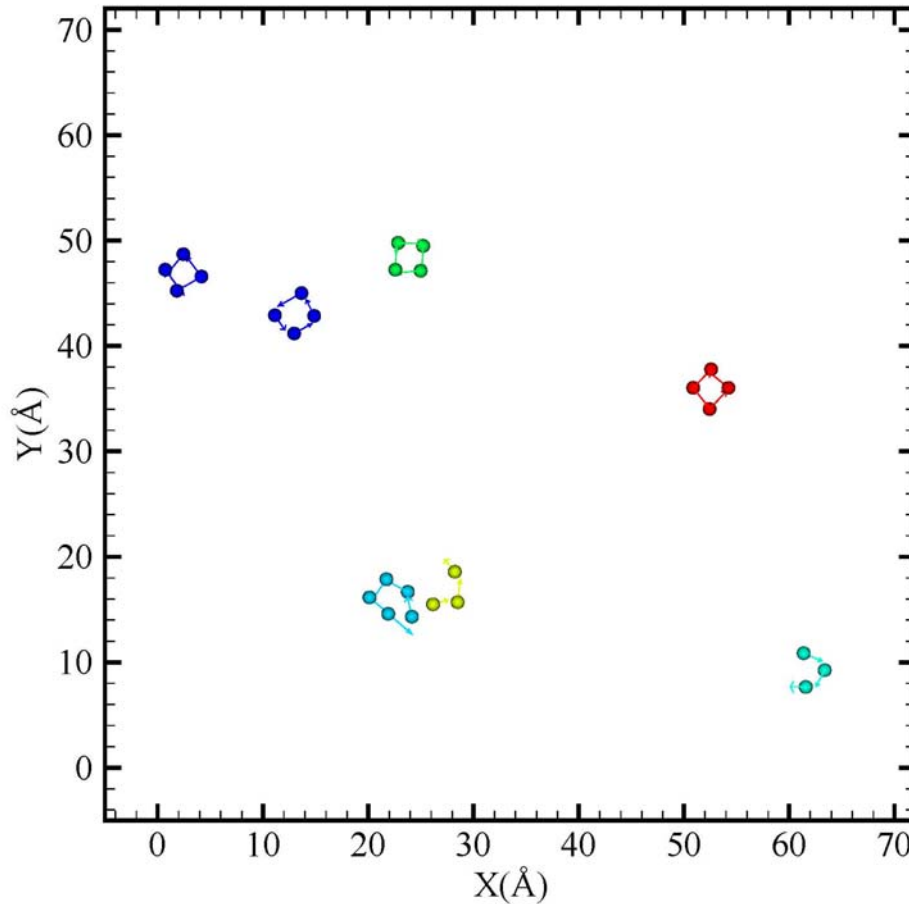


Figure 4.24 String-like motions captured in Stationary $\Sigma 5$ [001] twist boundary

In order to explore the nature of sting-like cooperative motions, we have

performed a series of controlled simulations in $\Sigma 5$, $\Sigma 13$ and general high-angle twist boundaries without applying external driving force at 900K. With the same technique, we found the existence of the similar string-like cooperative motions in all cases even though the grain boundaries were stationary, indicated in Figure 4.24; Figure 4.25 and Figure 4.26.

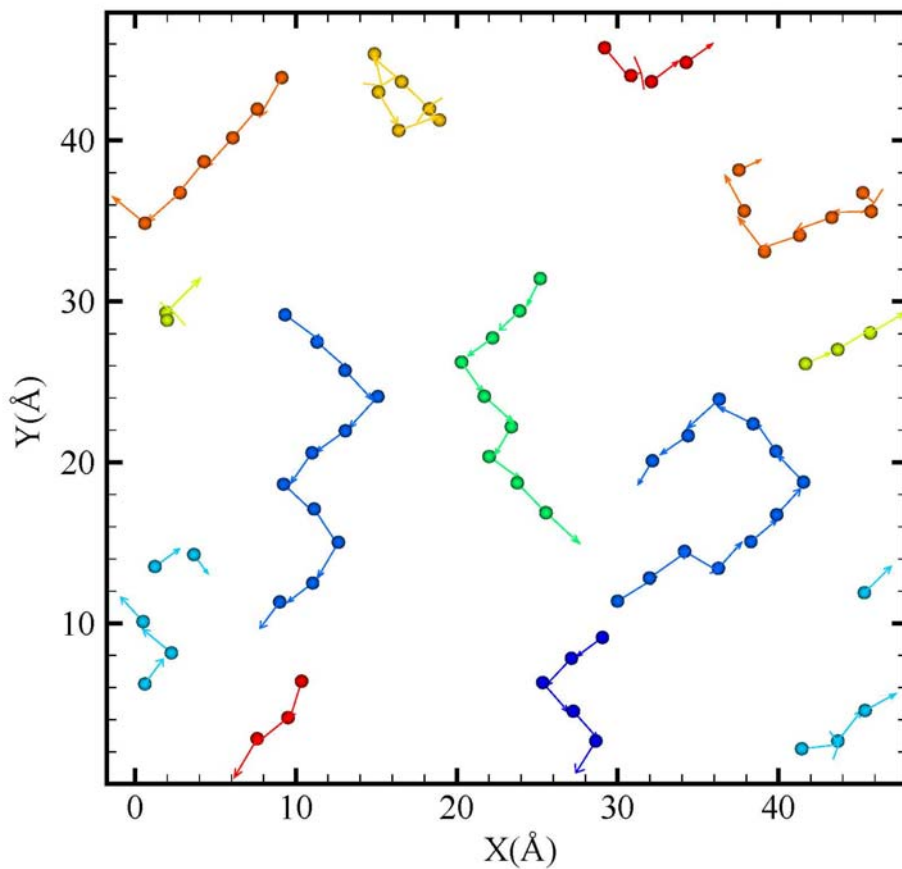


Figure 4.25 String-like motions captured in Stationary $\Sigma 13$ [001] twist boundary

Compared with the migrating grain boundaries, the average string length tended to be longer and the total population of strings seemed to be less in the stationary boundaries. These observations were consistent with our previous

findings of the string motion in tilt grain boundaries [41].

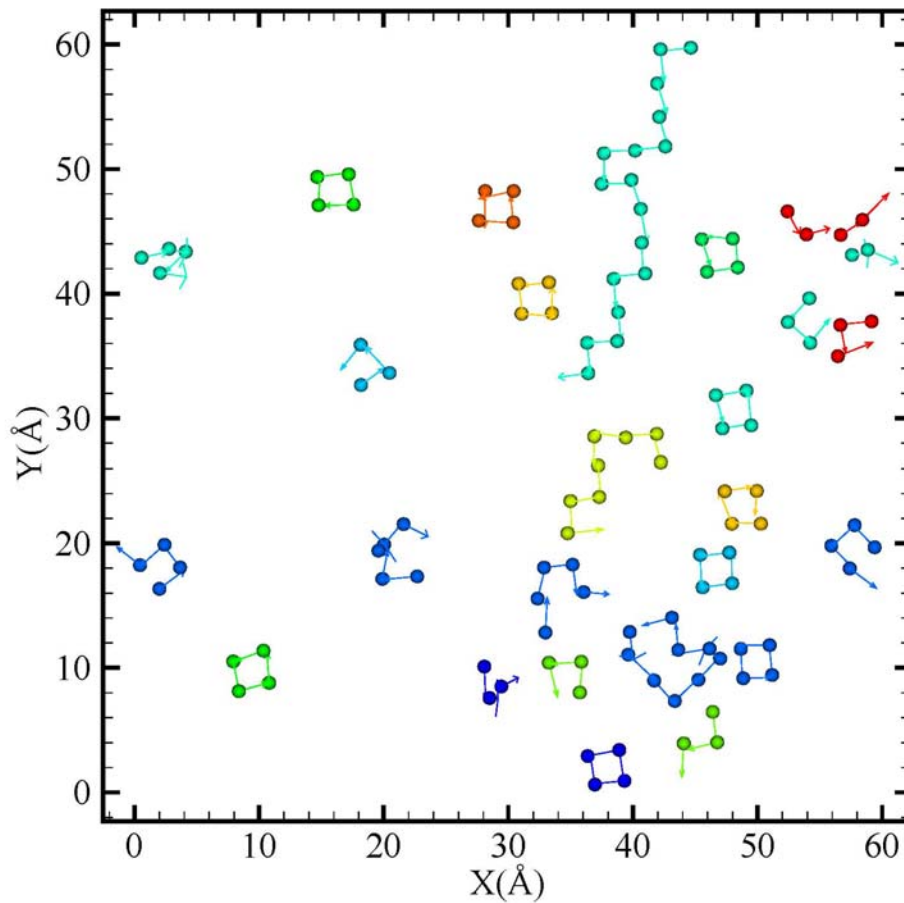


Figure 4.26 String-like motions captured in Stationary general [001] twist boundary

Interestingly, the special 4-atom shuffling motions were observed and predominant in the stationary $\Sigma 5$ twist boundary, shown in Figure 4.27. This suggests that the 4-atom shuffles are one of the intrinsic atomic motions in $\Sigma 5$ twist boundary. Hence, we can conclude that string-like cooperative motions (including 4-atom shuffles) are intrinsic atomic motions in twist grain boundaries and their behaviors depend greatly on the external conditions, such as stresses, impurities, temperatures, etc [64].

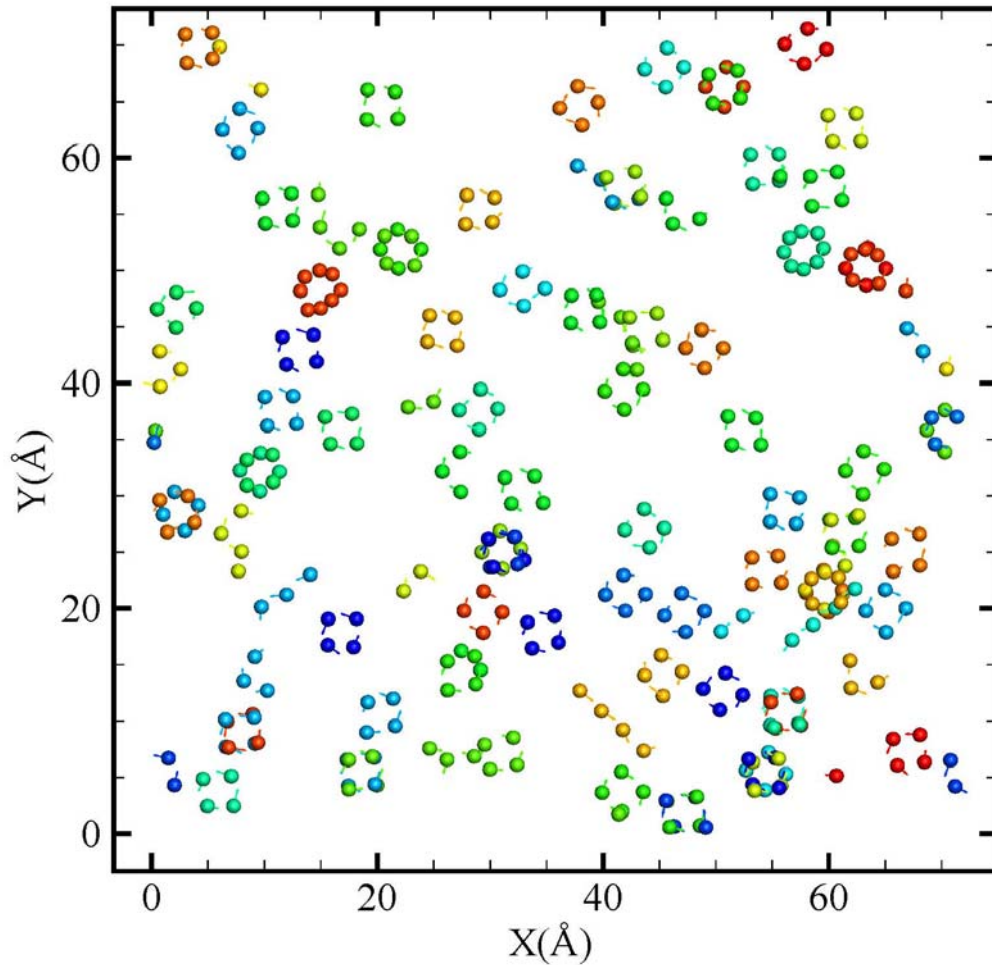


Figure 4.27 4-atom shuffling motion in stationary $\Sigma 5$ twist boundary

4.6 Simulation Result Discussions

One obvious question is how to relate the atomic mechanisms for grain boundary migration observed here to experimentally measurable quantities such as activation energy for migration. In particular, can we explain the variation of activation energy with misorientation in terms of atomic motions? Previous work [64] has established that the longer the average length of these strings presented, the larger the activation energies for grain boundary migration were. This finding

was in accordance with the Adams and Gibbs (AG) theory [68] of relaxation in glass forming liquids. Our previous atomistic simulations of grain boundary migration in general tilt boundary [40] suggested that the distribution of string lengths $P(n)$ was an approximately exponential function of n ,

$$P(n) \sim \exp(-n / \langle n \rangle), \quad (4.11)$$

where $\langle n \rangle$ is the average string length. Figure 4.28 shows the distribution of string lengths at $\Delta t = t^*$, where the string length $\bar{n}(\Delta t)$ exhibits a maximum during grain boundary migration for the $\Sigma 5$, $\Sigma 13$ and general twist boundaries. It is noted that the string with four members in both $\Sigma 5$ and general twist boundaries is more likely to be found in a grain boundary. This is consistent with the overall string-like cooperative motions shown in Figure 4.24 and Figure 4.26. Linear fitting of the data set yields the average string length $\langle n \rangle$ for the $\Sigma 5$, $\Sigma 13$, and general twist boundaries are 0.97, 3.07, and 1.89, respectively. The inset of Figure 4.28 plots the average string length $\langle n \rangle$ versus activation energy for migration Q for the three boundaries. The linear relationship between these two quantities is consistent with our previous findings in general tilt grain boundary [40] as well as the observations in glass-forming liquids [69-71]. It is also noted the average string length in the $\Sigma 5$ twist boundary is near unity. This implies that while individual strings can occur in $\Sigma 5$ twist boundary during migration, the string motions are indeed uncorrelated in a statistical sense.

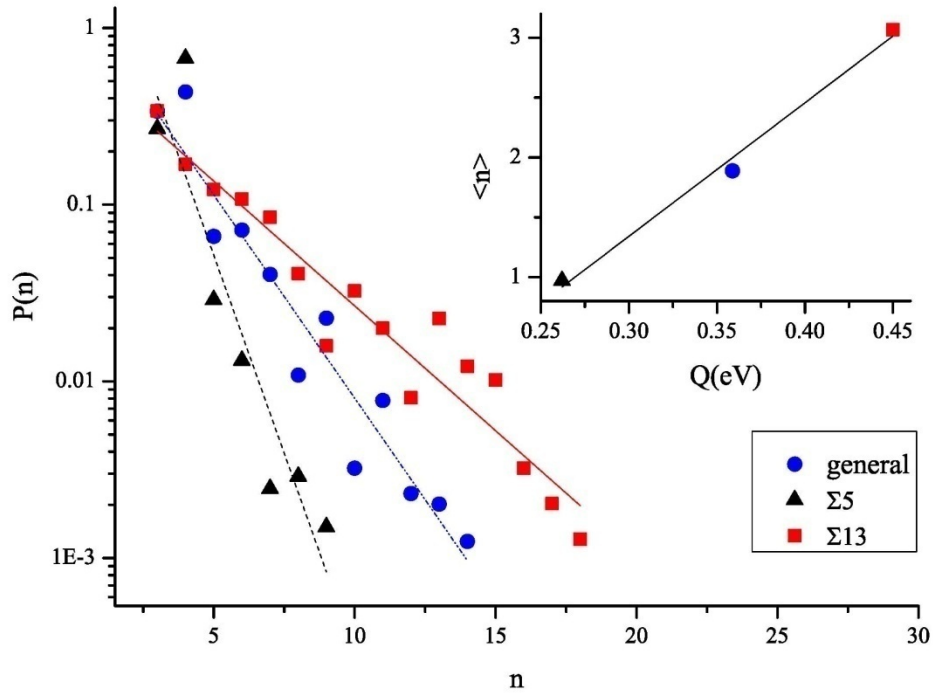


Figure 4.28 String-length distribution function $P(n)$ for $\Sigma 5$, $\Sigma 13$ and general high angle twist boundary at 900K. The inset shows the correlation between the average string length $\langle n \rangle$ and the activation energy for migration Q for three twist boundaries.

Up to this point, we have identified i) multi-atom collective jump (including general cooperative string motions in all boundaries and special 4-atom shuffle motions in $\Sigma 5$ boundary) and ii) single atom jump in all boundaries (including “short jump” in $\Sigma 13$ boundaries). Based upon these observations and analysis, we are now able to draw a picture of how the atomic motions lead to grain boundary migration in different twist boundaries.

(1) Since $\Sigma 5$ is the lowest possible CSL that can be obtained in the $[001]$ rotation

in the fcc metals, $\Sigma 5$ grain boundary possesses the highest local symmetry or order among all $[001]$ twist boundaries. Because of this, the atomistic migration mechanisms are relatively simple, i.e., 4-atom shuffling motions along DSC-lattice leads to grain orientation change from one to the other and this translation occurs within one (002) atomic plane. This finding is consistent with other reports [14, 42, 43]. However, our simulation also shows that correlation between each 4-atom shuffles is weak, suggesting that the migration is due to random 4-atom shuffles rather than the propagation of kinks along ledges (i.e., from one 4-atom shuffles to adjacent 4-atom shuffles).

(2) Although $\Sigma 13$ is the closest CSL to $\Sigma 5$ in the $[001]$ rotation in fcc metals, the atomic motions during migration in $\Sigma 13$ twist boundary exhibit significant difference from those in $\Sigma 5$ boundary. First of all, the $\Sigma 13$ string-like cooperative motions likely form a network within grain boundary plane [see Figure 4.21]. Additional analysis revealed that such a network is the representation of screw dislocation cores within grain boundary plane. String-like cooperative motions prefer to occur along these dislocation cores as they provide additional free volume. Meanwhile, no special 4-atom shuffling motions are observed in $\Sigma 13$ boundary. On the other hand, the “short jump” path in $\Sigma 13$ boundary is much more complicated than the path in $\Sigma 5$ boundary. Based on the atomic trajectories and the angular distribution

function, we can only characterize the single atom hops into inner and outer ring jump, rather than more specific paths. Since the “short jump” is mostly not correlated [See Figure 4.20], we believe that the single atom “short jump” is the dominant atomic motion that controls the grain to change from one orientation to the other. Enough evidence here also suggests that intensive string-like cooperative motions are important during migration since the dislocation network has pinning effect on the boundary motion.

- (3) Compared with the Σ twist boundaries, the string-like cooperative motions in general high angle twist boundary are predominant. Meanwhile the single atom hop in the general boundary does not exhibit any characteristic displacement that is less than an atomic distance, i.e., the single atom hop distance is close to the first nearest neighbor distance. These observations suggest that no well-defined short jump path exists in non- Σ boundary during migration, and both single atom hop and multi-atom jump are responsible for the orientation change from one crystal to the other.

Although in general the atomic motions that govern twist grain boundary migration can be characterized into single atom hop and multi-atom hop, the detailed atomistic mechanisms are sensitive to grain boundary orientation or grain boundary local symmetry. For CSL twist grain boundary, the “short jump” path becomes more complicated when the boundary change from low Σ to high Σ . boundary. This “short jump” will disappear when the boundaries change from

Σ boundary to non- Σ boundary. Meanwhile the string-like cooperative motion becomes increasingly important when Σ boundary switches to non- Σ boundary. On the other hand, the string-like cooperative motion will become predominant in low angle twist boundaries than in high angle twist boundaries since the presence of the well-defined screw dislocations. Therefore, atomistic mechanisms for twist grain boundary migration highly depend on the grain boundary structure. Similar observations can be also found in in-organic systems, where mobility of grain boundary migration is correlated to grain boundary structures [72].

4.7 Twist Boundary Migration Mechanism Study Conclusions

In the present thesis, we performed molecular dynamics simulations to identify the atomistic mechanisms by which grain boundaries migrate in a series of [001] twist grain boundaries. In particular, a $\theta=36.87^\circ \Sigma 5$, a $\theta=22.63^\circ \Sigma 13$ and a $\theta=40.23^\circ$ general twist boundaries driven by the stored elastic free energy were investigated. The simulation results of non-zero activation energy for the grain boundaries interest here confirmed that grain boundary migration in twist boundaries is a thermal activated process. Using quantitative string measurement, van Hove correlation function and angular distribution function, we were able to characterize the atomic motions during migration into multi-atom jump and single atom jump. Although the string-like cooperative motion were proved to be an intrinsic atomic motion, the activation energy for grain boundary migration was nicely correlated with the average string length, suggesting any factors such as

external stresses, temperature, impurities that can alter the nature of multi-atom collective motion will have effects on the activation energy for migration, in turn, they can greatly change the drifting velocity for boundary migration.

While our simulations of migration of $\Sigma 5$ twist boundary confirmed the existence of 4-atom shuffling motion, as reported by experiments and simulations [14, 42, 43], the migration of one (002) atomic plane is controlled by the random occurrence of 4-atom shuffling motion, rather than the propagation of kinks along ledges. Unlike in the case of the $\Sigma 5$ twist boundary, “short jumps” are mainly uncorrelated and the string-like cooperative motions in the $\Sigma 13$ twist boundary form a dislocation network in a statistical sense. Usually, it is difficult to visualize the dislocation cores within grain boundary when the misorientation angle is larger than 15° . However, the representation of string-like motions in “low” high angle twist boundaries provides us an alternative way to investigate grain boundary structures.

The present simulation results on the mechanism for grain boundary migration suggest a simple to complex mechanism transition when the grain boundary structure changes from low Σ boundary to high Σ boundary and further to general non- Σ boundary. In particular, boundary migration in $\Sigma 5$ twist boundary (low Σ boundary) is simply controlled by a special 4-atom shuffling motions and the “short jump” path is also relatively simple. Such a “short jump” path becomes more complicated in a $\Sigma 13$ boundary (higher Σ boundary) and completely

indistinguishable in a general high angle boundary. Meanwhile, the collective motions tend to form a more complicated screw dislocation network in a $\Sigma 13$ boundary and become almost random in the general high angle boundary.

Although in the present simulations, we have chosen different types (e.g., low angle and high angle, Σ and non- Σ) of twist grain boundaries to represent the typical boundaries that exist in nature, it is still very limited and only focuses on [001] twist boundaries. Therefore, it is not yet possible to prove the generality of these observations for all twist grain boundaries. However, the trend for the atomistic migration mechanisms change from low Σ to general boundary found in this work is consistent with the earlier prediction in [43]. Nonetheless, to the best of our knowledge, the present results represent the most complete systematic analysis of the atomistic mechanisms of twist grain boundary migration performed to date.

Chapter 5 Conclusions and Future Work

In this thesis, we have investigated a series of twist [001] grain boundary migration driven by the stored elastic energy using MD simulation. Temperature dependence of grain boundary mobility was obtained. Atomistic mechanisms for each selected twist boundary was thoroughly investigated. Correlations between the activation energy for grain boundary migration and the average string length was established.

Molecular Dynamics simulation was proved to be an effective alternative to quantitatively determine grain boundary mechanisms dependence on boundary misorientation, since detailed atomic motions during migration are readily accessible. Nevertheless, due to indefinite input atomic potentials, simulation results presented in this thesis could only be served as a supplement for real experiments.

Simulation was only carried out on fcc Ni in the present work, owing to its large elastic anisotropy. In order to obtain a universal grain boundary migration mechanism, simulations with other materials should be performed in future work. Achieving a general grain boundary migration mechanism, also, demands considering a variety of grain boundaries, i.e., tilt grain boundaries, mixed tilt-twist boundaries, symmetric boundaries and so forth.

Bibliography

- [1] Callister W. Materials Science and Engineering : An Introduction: Wiley, 2000.
- [2] Gottstein G, Shvindlerman LS. Grain Boundary Migration in Metals : Thermodynamics, Kkinetics, Applications. Boca Raton, FL.: CRC Press, 1999.
- [3] Porter DA, Easterling KE. Phase Transformations in Metals and Alloys, Second Edition, 1992.
- [4] Read WT. Dislocations in Crystals. McGraw-Hill, 1953.
- [5] Sutton AP, Vitek V. On the Structure of Tilt Grain-Boundaries in Cubic Metals .1. Symmetrical Tilt Boundaries. Philosophical Transactions of the Royal Society of London Series a-Mathematical Physical and Engineering Sciences 1983;309:1.
- [6] Pond RC, Smith DA. Absorption of Dislocations by Grain-Boundaries. Philos Mag 1977;36:353.
- [7] Upmanyu M, Srolovitz DJ, Lobkovsky AE, Warren JA, Carter WC. Simultaneous Grain Boundary Migration and Grain Rotation. Acta Mater 2006;54:1707.
- [8] Otsuki A, M. M. In Grain Boundary Structure and Related Phenomena. JIMIS-4: Grain Boundary Structure and Related Phenomena, Supplement to Transactions of Japan Institute of Metals 1986;27:789.
- [9] Read WT, Shockley W. Dislocation Models of Crystal Grain Boundaries. Phys Rev 1950;78:275.
- [10] Turnbull D. Theory of Grain Boundary Migration Rates. Journal of Metals

- 1951;3:661.
- [11] Gottstein G, Molodov DA, Shvindlerman LS. Grain Boundary Migration in Metals: Recent Developments. *Interface Science* 1998;6:7.
- [12] Winning M, Gottstein G, Shvindlerman LS. On the Mechanisms of Grain Boundary Migration. *Acta Mater* 2002;50:353.
- [13] Upmanyu M, Smith RW, Srolovitz DJ. Atomistic Simulation of Curvature Driven Grain Boundary Migration. *Interface Science* 1998;6:41.
- [14] Schonfelder B, Gottstein G, Shvindlerman LS. Comparative Study of Grain-Boundary Migration and Grain-Boundary Self-Diffusion of [001] Twist-Grain Boundaries in Copper by Atomistic Simulations. *Acta Mater* 2005;53:1597.
- [15] Schonfelder B, Wolf D, Phillpot SR, Furtkamp M. Molecular-Dynamics Method for the Simulation of Grain-Boundary Migration. *Interface Science* 1997;5:245.
- [16] Mullins WW. Magnetically Induced Grain-Boundary Motion in Bismuth. *Acta Metall Mater* 1956;4:421.
- [17] Zhang H, Mendeleev MI, Srolovitz DJ. Computer Simulation of The Elastically Driven Migration of a Flat grain boundary. *Acta Mater* 2004;52:2569.
- [18] Sheikh-Ali AD, Molodov DA, Garmestani H. Boundary Migration in Zn Bicrystal Induced by a High Magnetic Field. *Applied Physics Letters* 2003;82:3005.
- [19] Winning M. Strain-Induced Migration of Tilt Grain Boundaries. *Scripta Materialia* 2008;58:85.

- [20] Rath BB, Hu H. Effect of Driving Force on Migration of High-Angle Tilt Grain Boundaries in Aluminum Bicrystals. Transactions of the Metallurgical Society of Aime 1969;245:1577.
- [21] Rath BB, Hu H. Driving-Force Dependence of Rate of Boundary Migration in Zone-Refined Aluminum Crystals. Transactions of the Metallurgical Society of Aime 1969;245:1243.
- [22] Rath BB, Hu H. Anisotropy of Grain Boundary Mobility in Zone-Refined Aluminum Crystals. Transactions of the Metallurgical Society of Aime 1966;236:1193.
- [23] Sun RC, Bauer CL. Tilt Boundary Migration in Nacl Bicrystals. Acta Metall Mater 1970;18:639.
- [24] Sun RC, Bauer CL. Measurement of Grain Boundary Mobilities Through Magnification of Capillary Forces. Acta Metall Mater 1970;18:635.
- [25] Aristov VY, Fridman EM, Shvindlerman LS. Boundaries Migration in Aluminum Bicrystals. Fizika Metallov I Metallovedenie 1973;35:859.
- [26] Gottstein G, Shvindlerman LS. On The True Dependence of Grain-Boundary Migration Rate on Driving Force. Scripta Metallurgica Et Materialia 1992;27:1521.
- [27] Cole DG, Feltham P, Gillam E. On the Mechanism of Grain Growth in Metals, with Special Reference to Steel. Proceedings of the Physical Society of London Section B 1954;67:131.
- [28] Gottstein G, Molodov DA, Czubayko U, Shvindlerman LS. High-Angle

Grain-Boundary Migration in Aluminum Bicrystals. 1995. p.89.

- [29] Aust KT, Rutter JW. Temperature Dependence of Grain Migration in High-Purity Lead Containing Small Additions of Tin. Transactions of the American Institute of Mining and Metallurgical Engineers 1959;215:820.
- [30] Molodov DA, Straumal BB, Shvindlerman LS. The Effect of Pressure on Migration of (001) Tilt Grain-Boundaries in Tin Bicrystals. Scripta Metallurgica 1984;18:207.
- [31] Molodov DA, Czubayko U, Gottstein G, Shvindlerman LS. Mobility of [111] Tilt Grain-Boundaries in the Vicinity of the Special Misorientation $\Sigma=7$ In Bicrystals of Pure Aluminum. Scripta Metallurgica et Materialia 1995;32:529.
- [32] Kopetskii CV, Sursaeva VG, Shvindlerman LS. Activationless Motion of Grain-Boundaries in Zinc. Fizika Tverdogo Tela 1979;21:401.
- [33] Lucke K, Detert K. A Quantitative Theory of Grain-Boundary Motion and Recrystallization in Metals in the Presence of Impurities. Acta Metall Mater 1957;5:628.
- [34] Cahn JW. Impurity-Drag Effect in Grain Boundary Motion. Acta Metall Mater 1962;10:789.
- [35] Zhang H, Upmanyu N, Srolovitz DJ. Curvature Driven Grain Boundary Migration in Aluminum: Molecular Dynamics Simulations. Acta Mater 2005;53:79.
- [36] Foiles SM, Baskes MI, Daw MS. Embedded-Atom-Method Functions for the Fcc Metals Cu, Ag, Au, Ni, Pd, Pt, and Their Alloys. Phys Rev B 1986;33:7983.
- [37] Janssens KGF, Olmsted D, Holm EA, Foiles SM, Plimpton SJ, Derlet PM.

- Computing the Mobility of Grain Noundaries. *Nat. Mater.* 2006;5:124.
- [38] Trautt ZT, Upmanyu M, Karma A. Interface Mobility from Interface Random Walk. *Science* 2006;314:632.
- [39] Zhang H, Srolovitz DJ. Simulation and Analysis of the Migration Mechanism of Sigma 5 Tilt Grain Boundaries in an Fcc Metal. *Acta Mater* 2006;54:623.
- [40] Zhang H, Srolovitz DJ, Douglas JF, Warren JA. Atomic Motion During the Migration of General [001] Tilt Grain Goundaries in Ni. *Acta Mater* 2007;55:4527.
- [41] Zhang H, Srolovitz DJ, Douglas JF, Warren JA. Characterization of Atomic Motion Governing Grain Boundary Migration. *Phys Rev B* 2006;74.
- [42] Jhan RJ, Bristowe PD. A Molecular-Dynamics Study of Grain-Boundary Migration without the Participation of Secondary Grain-Boundary Dislocations. *Scripta Metallurgica Et Materialia* 1990;24:1313.
- [43] Babcock SE, Balluffi RW. Grain-Boundary Kinetics 2. Insitu Observations of the Role of Grain-Boundary Dislocations in High-Angle Boundary Migration. *Acta Metall Mater* 1989;37:2367.
- [44] Mendeleev MI, Zhang H, Srolovitz DJ. Grain Boundary Self-Diffusion in Ni: Effect of Boundary Inclination. *Journal of Materials Research* 2005;20:1146.
- [45] Mott NF. Slip at Grain Boundaries and Grain Growth in Metals. *P Phys Soc Lond* 1948;60:391.
- [46] R.C.Gifkins. Development of the Island Model for Grain Boundaries. *Physical Metallurgy Section C.S.I.R.O* 1967.

- [47] Krakow W. Structural Multiplicity Observed at A $\Sigma=5$ /[001] 53.1-Degrees Tilt Boundary in Gold. *Philos Mag A* 1991;63:233.
- [48] Gleiter H. Mechanism of Grain Boundary Migration. *Acta Metall Mater* 1969;17:565.
- [49] Kvam EP, Balluffi RW. Observations of Hierarchical Grain-Boundary Dislocation-Structures in [001] Symmetrical Tilt Boundaries in Gold. *Philos Mag A* 1987;56:137.
- [50] Babcock SE, Balluffi RW. Grain-Boundary Kinetics .1. In situ Observations of Coupled Grain-Boundary Dislocations-Motion, Crystal Translation and Boundary Displacement. *Acta Metall Mater* 1989;37:2357.
- [51] Bishop GH, Harrison RJ, Kwok T, Yip S. Computer Molecular-Dynamics Studies of Grain-Boundary Structures .1. Observations of Coupled Sliding and Migration in a 3-Dimensional Simulation. *J Appl Phys* 1982;53:5596.
- [52] Cahn JW, Mishin Y, Suzuki A. Coupling Grain Boundary Motion to Shear Deformation. *Acta Mater* 2006;54:4953.
- [53] Alder BJ, Wainwright TE. PHASE TRANSITION FOR A HARD SPHERE SYSTEM. *J Chem Phys* 1957;27:1208.
- [54] Alder BJ, Wainwright TE. Studies in Molecular Dynamics .1. General Method. *J Chem Phys* 1959;31:459.
- [55] Gibson JB, Goland AN, Milgram M, Vineyard GH. Dynamics of Radiation Damage. *Phys Rev* 1960;120:1229.

- [56] Rahman A. Correlations in Motion of Atoms In Liquid Argon. Physical Review a-General Physics 1964;136:A405.
- [57] Verlet L. Computer Experiments on Classical Fluids .I. Thermodynamical Properties of Lennard-Jones Molecules. Phys Rev 1967;159:98.
- [58] Verlet L. Computer Experiments on Classical Fluids .2. Equilibrium Correlations Functions. Phys Rev 1968;165:201.
- [59] Andersen H. Molecular-Dynamics Simulations at Constant Pressure and-or Temperature. J Chem Phys 1980;72:2384.
- [60] Nosé S. A Unified Formulation of the Constant Temperature Molecular-Dynamics Methods. J Chem Phys 1984;81:511.
- [61] Hoover W, Holian B. Kinetic Moments Method for the Canonical Ensemble Distribution. Physical Review a-General Physics 1996;211:253.
- [62] Voter AF, Chen SP. in Accurate Interatomic Potentials for Ni, Al and Ni₃Al. Materials Research Society Symposia Proceedings 1987;82:175.
- [63] S.J.Plimpton. Fast Parrallel Algorithms for Short-Range Molecular Dynamics. Journal of Computational Physics 1995;117:1.
- [64] Zhang H, Srolovitz DJ, Douglas JF, J.A. W. Grain Boundaries Exhibit the Dynamics of Glass-Forming Liquids. Proceedings of the National Academy of Sciences of the United States of America 2009;106:7729.
- [65] Zhang H, Mendeleev MI, Srolovitz DJ. Mobility of Sigma 5 Tilt Grain Boundaries: Inclination Dependence. Scripta Materialia 2005;52:1193.

- [66] Gottstein G, Shvindlerman LS. The Compensation Effect in Thermally Activated Interface Processes. *Interface Science* 1998;6:265.
- [67] Amelinckx S, Dekeyser W. The Structure and Properties of Grain Boundaries. *Solid State Phys* 1959;8:325.
- [68] Adam G, Gibbs JH. On Temperature Dependence of Cooperative Relaxation Properties in Glass-Forming Liquids. *J Chem Phys* 1965;43:139.
- [69] Douglas JF, Dudowicz J, Freed KF. Does Equilibrium Polymerization Describe the Dynamic Heterogeneity of Glass-Forming Liquids? *J Chem Phys* 2006;125:144907.
- [70] Riggleman RA, Yoshimoto K, Douglas JF, de Pablo JJ. Influence of Confinement on the Fragility of Antiplasticized and Pure Polymer Films. *Physical Review Letter* 2006;97:045502.
- [71] Donati C, Douglas JF, Kob W, S.J. P, Poole PH, Glotzer SC. Stringlike Cooperative Motion in a Supercooled Liquid. *Physical Review Letter* 1998;80:2338.
- [72] Dillon SJ, Harmer MP. Multiple Grain Boundary Transitions in Ceramics: A case Study of Alumina. *Acta Mater* 2007;55:5247.